



HAL
open science

GABAB Receptors Tune Cortical Feedback to the Olfactory Bulb.

Camille Mazo, Gabriel Lepousez, Antoine Nissant, Matthew T Valley,
Pierre-Marie Lledo

► **To cite this version:**

Camille Mazo, Gabriel Lepousez, Antoine Nissant, Matthew T Valley, Pierre-Marie Lledo. GABAB Receptors Tune Cortical Feedback to the Olfactory Bulb.. Journal of Neuroscience, 2016, 10.1523/JNEUROSCI.3823-15.2016 . pasteur-01494505

HAL Id: pasteur-01494505

<https://pasteur.hal.science/pasteur-01494505>

Submitted on 23 Mar 2017

HAL is a multi-disciplinary open access archive for the deposit and dissemination of scientific research documents, whether they are published or not. The documents may come from teaching and research institutions in France or abroad, or from public or private research centers.

L'archive ouverte pluridisciplinaire **HAL**, est destinée au dépôt et à la diffusion de documents scientifiques de niveau recherche, publiés ou non, émanant des établissements d'enseignement et de recherche français ou étrangers, des laboratoires publics ou privés.

GABA_B Receptors Tune Cortical Feedback to the Olfactory Bulb

 Camille Mazo, Gabriel Lepousez, Antoine Nissant, Matthew T. Valley, and Pierre-Marie Lledo

Laboratory for Perception and Memory, Institut Pasteur, F-75015 Paris, France, and Centre National de la Recherche Scientifique, Unité Mixte de Recherche 3571, F-75015 Paris, France

Sensory perception emerges from the confluence of sensory inputs that encode the composition of external environment and top-down feedback that conveys information from higher brain centers. In olfaction, sensory input activity is initially processed in the olfactory bulb (OB), serving as the first central relay before being transferred to the olfactory cortex. In addition, the OB receives dense connectivity from feedback projections, so the OB has the capacity to implement a wide array of sensory neuronal computation. However, little is known about the impact and the regulation of this cortical feedback. Here, we describe a novel mechanism to gate glutamatergic feedback selectively from the anterior olfactory cortex (AOC) to the OB. Combining *in vitro* and *in vivo* electrophysiological recordings, optogenetics, and fiber-photometry-based calcium imaging applied to wild-type and conditional transgenic mice, we explore the functional consequences of circuit-specific GABA type-B receptor (GABA_BR) manipulation. We found that activation of presynaptic GABA_BRs specifically depresses synaptic transmission from the AOC to OB inhibitory interneurons, but spares direct excitation to principal neurons. As a consequence, feedforward inhibition of spontaneous and odor-evoked activity of principal neurons is diminished. We also show that tunable cortico-bulbar feedback is critical for generating beta, but not gamma, OB oscillations. Together, these results show that GABA_BRs on cortico-bulbar afferents gate excitatory transmission in a target-specific manner and thus shape how the OB integrates sensory inputs and top-down information.

Key words: feedforward inhibition; olfaction; oscillations; sensory circuits; synapse; top-down

Significance Statement

The olfactory bulb (OB) receives top-down inputs from the olfactory cortex that produce direct excitation and feedforward inhibition onto mitral and tufted cells, the principal neurons. The functional role of this feedback and the mechanisms regulating the balance of feedback excitation and inhibition remain unknown. We found that GABA_B receptors are expressed in cortico-bulbar axons that synapse on granule cells and receptor activation reduces the feedforward inhibition of spontaneous and odor-driven mitral and tufted cells' firing activity. In contrast, direct excitatory inputs to these principal neurons remain unchanged. This study demonstrates that activation of GABA_B receptors biases the excitation/inhibition balance provided by cortical inputs to the OB, leading to profound effects on early stages of sensory information processing.

Introduction

Sensory systems use prior experience and expectation to interpret the outside world. The integration of external information re-

quires combining the bottom-up flow of sensory information with top-down signals from higher brain areas. In the olfactory system, odorant information from sensory neurons are first integrated in the main olfactory bulb (OB) before broadcasting to the olfactory cortex through OB principal cells, the so-called mitral and tufted (M/T) cells (Poo and Isaacson, 2009; Franks et al., 2011). In turn, the olfactory cortex, and mainly the anterior piriform cortex and anterior olfactory nucleus (respectively APC and AON, collectively called the anterior olfactory cortex, AOC),

Received Oct. 20, 2015; revised June 4, 2016; accepted June 9, 2016.

Author contributions: C.M., G.L., M.T.V., and P.-M.L. designed research; C.M., G.L., A.N., and M.T.V. performed research; C.M., A.N., and M.T.V. analyzed data; C.M., G.L., and P.-M.L. wrote the paper.

This work was supported by the life insurance company AG2R-La-Mondiale, the Agence Nationale de la Recherche (ANR-15-CE37-0004), and the Laboratoire d'Excellence Revive (Investissement d'Avenir, ANR-10-LABX-73). Our laboratory is part of the Ecole des Neurosciences de Paris (ENP) Ile-de-France network and is affiliated with the Bio-Psy Laboratory of Excellence. C.M. is a recipient of a fellowship from the French Ministère de l'Éducation Nationale et de la Recherche. We thank Carine Moigneu and Laurent Cotter for viral injections; all members of the Lledo laboratory for their insights during the course of these experiments; Kurt Sailor for editing the manuscript; Manuel Mamelì for helpful discussions; Bernhard Bettler for providing GABAB^{fllox/flox} mice; Anne Lanjuin and Catherine Dulac for the Tbet-Cre mice; Karl Deisseroth and Edward Boyden for optogenetic tools; Gaël Moneron for help in setting up the fiber photometry path and the Genetically-Encoded Neuronal Indicator and Effector (GENIE) Project; and the Janelia Farm Research Campus of the Howard Hughes Medical Institute for sharing GCaMP6f constructs.

The authors declare no competing financial interests.

M.T. Valley's present address: Allen Institute for Brain Science, 601 Westlake Ave. N, Seattle, WA 98109.

Correspondence should be addressed to Pierre-Marie Lledo, Laboratory for Perception and Memory, Institut Pasteur and CNRS, 25 rue du Dr. Roux, 75 724 Paris Cedex 15, France. E-mail: pmlledo@pasteur.fr.

DOI:10.1523/JNEUROSCI.3823-15.2016

Copyright © 2016 the authors 0270-6474/16/368289-16\$15.00/0

projects back to the OB (Haberly and Price, 1978a, 1978b; Davis and Macrides, 1981). Cortico-bulbar projections mostly synapse with axonless OB interneuron granule cells (GCs) and, to a lesser extent, with M/T cells. This glutamatergic input onto GC proximal dendrites initiates action potentials and mediates feedforward inhibition onto M/T cells (Balu et al., 2007). In addition, GCs receive glutamatergic input from M/T cells on their apical dendrites, triggering locally reciprocal GABA release back onto M/T cells, thereby producing recurrent or lateral inhibition (Isaacson and Strowbridge, 1998).

In addition to the great number of glutamatergic cortico-bulbar inputs from the AOC, the OB also receives top-down inputs from neuromodulatory centers, including serotonergic fibers from the raphe, noradrenergic fibers from the locus coeruleus, and cholinergic and GABAergic fibers from the basal forebrain (Matsutani and Yamamoto, 2008; Linster and Fontanini, 2014). Given the abundance and diversity of top-down inputs to the OB and their strong impact on OB functions (Shea et al., 2008; Petzold et al., 2009; Boyd et al., 2012; Ma and Luo, 2012; Markopoulos et al., 2012; Soria-Gómez et al., 2014), deciphering how these inputs are modulated is essential to understanding their physiological role and how they regulate the OB network.

In this study, we demonstrate that GABA_B receptors (GABA_BRs), G-protein-coupled receptors of GABA, regulate specific cortico-bulbar excitatory synaptic transmission. Using conditional genetics to selectively knock out GABA_BR expression in the AOC, together with a combination of *in vitro* and *in vivo* electrophysiology, optogenetics, and fiber-photometry-based calcium imaging, we characterized the functional role of GABA_BR modulation at cortico-bulbar terminals. We show that presynaptic activation of GABA_BRs strongly depresses the AOC-to-GC synapse, resulting in diminished feedforward inhibition onto M/T cells' spontaneous and odor-evoked activity. However, the direct AOC-to-M/T cell excitation remains unchanged. In addition, activation of GABA_BRs also reduces OB spontaneous beta oscillations (15–40 Hz). Collectively, these data uncover a mechanism by which the cortical top-down influence to the OB can be refined precisely.

Materials and Methods

Animals

Adult wild-type (WT) C57BL/6RJ, GABA_B(1)^{fl/fl} (Haller et al., 2004), and Tbet-Cre (Haddad et al., 2013) male mice (maintained on a C57BL/6RJ background; 2–5 months old at the time of injection) were used in the study. This work was performed in compliance with the French application of the European Communities Council Directive of September 22, 2010 (2010/63/EEC) and approved by the local ethics committee (CETEA 89, project #01126.02).

Viral injection

Adeno-associated virus [AAV; capsid serotype 2/9 for Channelrhodopsin-2 (ChR2), ChRimson, and Cre viruses, and 2/1 for GCaMP6f] were generated by the Penn Vector Core or produced by the Institut National de la Santé et de la Recherche Médicale (INSERM, UMR 1089, IRT1 Vector platform Nantes, www.atlantic-gene-therapies.fr) from ChR2- (K. Deisseroth; catalog #26969 and #20297; Addgene), ChRimson- (E. Boyden; catalog #62723; Addgene), Cre recombinase-, or GCaMP6f (Penn Vector Core)-encoding plasmids. For electrophysiology experiments, high-titer stock of AAV containing the CaMKIIa-hChR2(H134R)-eYFP-WPRE construct (viral titer, 9.4×10^{12} genome copies per milliliter, $n = 14$ mice for *in vitro* recordings, $n = 15$ for *in vivo* recordings) or a 1:6 mixture of an AAV containing CaMKII-Cre-WPRE (viral titer, 1.1×10^{14}) and an AAV containing EF1a-DIO-hChR2(H134R)-mCherry-WPRE (viral titer, 1.4×10^{13}) were injected in WT ($n = 5$) and age-matched GABA_B(1)^{fl/fl} mice ($n = 4$). A separate cohort of animals were also injected with an AAV containing hSyn-

hChR2(H134R)-mCherry-WPRE [$n = 3$ for *in vitro* recordings, $n = 5$ for *in vivo* field EPSP (fEPSP) characterization solely]. No significant difference between using the Syn or CaMKIIa promoter was seen and results were pooled. For photometry experiments, high-titer stock of AAV containing the hSyn-ChRimson-TdTomato-WPRE (viral titer, 2.2×10^{13}) or hSyn-DIO-GCaMP6f-WPRE construct (viral titer: 1.1×10^{13}) were injected in Tbet-Cre mice ($n = 15$ odor-recording pairs from 2 mice). For viral injections, mice were deeply anesthetized with a ketamine and xylazine mixture (150 mg/kg Imalgene and 5 mg/kg Rompun, respectively, i.p.) and placed in a stereotaxic apparatus. A small craniotomy was performed and viral solution was injected into the AOC (stereotaxic coordinates: 2.1 mm anterior from bregma, 1.9 mm lateral, and at a depth of 3.3 and 3.7 mm from the brain surface; 150–200 nl/site, 300–400 nl total), allowing virus diffusion in the anterior APC and latero-posterior AON, or into the OB (AP: 5 mm, ML: 1.7 mm, DV: 0.7–1.5 mm, 300 nL total) through a glass micropipette attached to a Nanoinjector system (Nanoject II).

Electrophysiology

Slice recording. Tissue preparation was performed as described in Valley et al. (2013). Briefly, tissue was dissected in artificial CSF (ACSF) and 300- μ m-thick slices were vibrosectioned. Recordings were made with borosilicate glass pipettes with a tip resistance between 3 and 6 M Ω . Recordings were discarded if the access resistance exceeded half the input resistance of the cell or if the access resistance varied by $\sim 30\%$ during the experiment. Data were digitized at 10 kHz (EPC9double; HEKA). ChR2 stimulation used a 470 nm light-emitting diode array (Bridgelux). Light duration was controlled using a digital Sequencer (Master-8; A.M.P.I.) and all stimulations were given with an interstimulus interval of 20 s.

In vivo recording. Awake recordings were performed as described previously (Lepousez and Lledo, 2013; Soria-Gómez et al., 2014). Mice were anesthetized and an L-shaped metal bar and a silver reference electrode were fixed to the caudal part of the skull. Optic fibers [multimode, 430 μ m diameter, numerical aperture (NA) 0.39, Thorlabs] were bilaterally implanted above the anterior commissure (400 μ m posterior to the sinus of the olfactory bulb, 0.9 mm lateral, and at a depth of 2.3 mm from the brain surface with an angle of $\sim 30^\circ$). After 1 week of recovery, mice were slowly and progressively trained for head restraint habituation and a 5% sucrose solution was given as a reward. The craniotomy was performed the day before recording and protected with silicone sealant (KwikCast). An array of 4 tungsten electrodes (~ 3 M Ω ; FHC) glued to one or two miniature cannulas (polyimide tubing, 0.0035 inch, Neuralynx; positioned 100–200 μ m above the electrode tips, connected to a 10 μ l Hamilton syringe) was slowly lowered into the OB and a drop of silicone sealant was applied to the brain surface to increase recording stability. Both LFP and spiking signals were continuously recorded 40 min before and 60 min after local drug microinjection through the miniature cannula (injection speed: 0.05 μ l/min; 0.15–0.3 μ l total). Signals were pre-amplified (HS-18; Neuralynx), amplified (1000 \times ; Lynx8, Neuralynx) and digitized at 20 kHz (Power 1401 A/D interface; CED). The identity of M/T cells units were established on the basis of several criteria: (1) stereotaxic coordinates of the mitral cell layer; (2) decrease in both gamma oscillation amplitude and light-evoked fEPSP in the mitral cell layer compared with the LFP recorded in the GC layer (GCL) or external plexiform layer (EPL), where the current sources/sinks are localized (Neville and Haberly, 2003); (3) increase in background spiking activity in a narrow band of 100–150 μ m; (4) typical spontaneous activity patterns coarsely time locked to the respiration rhythm; and (5) odor-evoked responses. Light stimulation of AOC axons was performed using either an optic fiber placed on the OB brain surface or with implanted optic fibers coupled to a DPSS laser (473 nm, 150 mW; CNI Lasers; output fiber intensity, 20 mW) via a custom-built fiber launcher and controlled by a PS-H-LED laser driver connected to the CED interface. Light stimulation consisted in single, paired (40 Hz), or train stimulation (10–100 Hz) of 5-ms-long light pulses. The respiration signal was recorded using a thermocouple (0.005 inch Teflon-coated thermocouple, 5TC-TT-JI-40-1M; Omega) placed in front of the animal's nostril, amplified (10,000 \times), and band-pass filtered (0–10 Hz). The craniotomy

was cleaned and covered with Kwik-Cast between sessions. Four recording sessions per mouse (2 per hemisphere) were made at least 1–2 d apart.

Characterization of the light-evoked fEPSP (see Fig. 2*B,C*) was performed in anesthetized mice. Animals were anesthetized using ketamine/xylazine and positioned in a stereotaxic frame. The animal's body temperature was maintained at 37.5°C by a heating pad and the respiration was monitored to control the anesthesia. LFP recordings were then performed as described above.

Odor presentation. We used a custom-built flow-dilution olfactometer controlled by the CED interface. Pure monomolecular odorants (Sigma-Aldrich) were diluted in mineral oil (10%) in odorless glass vial. Saturated odor vapor was further diluted with humidified clean air (1:10) by means of computer-controlled solenoid pinch valves. Odor presentation dynamics were monitored and calibrated using a mini-photoionization detector (mini-PID, Aurora). Cycles of odor, light, and odor + light presentations were repeated at least seven times for each condition. Stimuli were applied for 1 s and a given odorant was presented every 50 s to reduce sensory adaptation. The odorants used in the final dataset were as follows: valeraldehyde ($n = 11$ responses), acetophenone ($n = 5$), butyric acid ($n = 3$), 2-hexanone ($n = 3$), (S)-limonene ($n = 3$), ethyl tiglate ($n = 2$), ethyl butyrate ($n = 1$), ethyl valerate ($n = 1$), and 1,4 cineole ($n = 1$) and a binary (1:1) mixture of 1-pentanol and 1,4 cineole ($n = 4$), ethyl butyrate and ethyl valerate ($n = 4$), valeraldehyde and ethyl tiglate ($n = 1$), (S)-limonene and 2-hexanone ($n = 1$).

Calcium imaging using fiber photometry

A fiber photometry system adapted from Gunaydin et al. (2014) was used (see Fig. 7*A*). Immediately after GCaMP6f virus injection in the OB, optic fibers (multimode, 430 μm diameter, NA 0.48, LC zirconia ferrule) were implanted bilaterally in the dorsolateral part of the OB above the virus injection site. Three weeks after injection, GCaMP6f was excited continuously using a 473 nm DPSS laser (output fiber intensity, 0.4–0.5 mW; CNI Lasers) reflected on a dichroic mirror (452–490 nm/505–800 nm) and collimated into a 400 μm multimode optic fiber (NA 0.48) with a convergent lens ($f = 30$ mm). The emitted fluorescence was collected in the same fiber and transmitted by the dichroic mirror, filtered (525 ± 19 nm), and focused on a NewFocus 2151 femtowatt photoreceptor (Newport; DC mode). Reflected blue light along the light path was also measured with a second amplifying photodetector (PDA36A; Thorlabs) to monitor light excitation and fiber coupling. Signals from both photodetectors were digitized by a digital-to-analog converter (Power 1401; CED) at 5000 Hz and recorded using Spike2 software. For AOC stimulation using ChRimson, an optic fiber (multimode, 430 μm diameter, NA 0.39, with LC zirconia ferrule; Thorlabs; 5–10 mW output fiber intensity) were implanted bilaterally above the AOC and connected to a DPSS laser (589 nm, 200 mW; CNI Lasers) via a custom-built fiber launcher. For drug injection, bilateral acute intrabulbar injections were done through implanted guide cannulas (injection volume, 0.5 μl ; speed, 0.1 $\mu\text{l}/\text{min}$ via a 33-gauge cannula connected to a 10 μl Hamilton syringe). For odor presentation, mice were placed in a small, ventilated cage (~0.5 L). Pure monomolecular odorants (Sigma-Aldrich) were diluted in mineral oil (1%) in an odorless glass vial and saturated odor vapor was delivered directly into the ventilated cage at a flow rate of 3 L/min. Odors were presented every 30 s and odor presentation dynamics in the cage were monitored constantly using a mini-PID (Aurora). The odorants used in the final dataset were as follows: valeraldehyde ($n = 3$), ethyl tiglate ($n = 3$), pentyl acetate ($n = 3$), ethyl valerate ($n = 2$), 2-hexanone ($n = 1$), ethyl butyrate ($n = 1$), linalool ($n = 1$), and pentanol ($n = 1$).

Pharmacology

Lidocaine (2-diethylamino-*N*-(2,6-dimethylphenyl)acetamide, 2% *in vivo*), NBQX (2,3-dioxo-6-nitro-1,2,3,4-tetrahydrobenzo[*f*]quinoxaline-7-sulfonamide; 1 mM *in vivo*), baclofen ((*RS*)-4-Amino-3-(4-chlorophenyl)butanoic acid; 250 μM in slice and 2.5 mM for *in vivo* experiments), and CGP 52432 ([3-[[[(3,4-dichlorophenyl)methyl]amino]propyl] (diethoxymethyl)phosphinic acid; 10 μM for slice and 100 μM for *in vivo* recording) were obtained from Sigma-Aldrich or Tocris Bioscience and dissolved at a final concentration in either sterile saline for *in vivo* experiments or ACSF for slice experiments. Analyzing the changes in fEPSPs at different depths in the GCL

after baclofen injections allowed an estimation of the drug diffusion to be <500–600 μm (see “Results” section).

Histology

For postrecording histological analysis of electrode positioning and ChR2 expression, animals were intracardially perfused [4% paraformaldehyde (PFA) in 0.1 M phosphate buffer] and the brains were removed and postfixed in the same fixative overnight. Sixty-micrometer-thick brain sections were cut on a vibratome, rinsed in PBS, counterstained with the nuclear dye 4,6-diamidino-2-phenylindole (DAPI), and mounted on slides. Viral expression at the injection site was confirmed and OB sections were inspected to check for proper axonal expression, absence of virus diffusion into the OB, and the absence of significant somatic labeling in the OB. To amplify the eYFP fluorescent signal, immunohistochemistry was performed with a chicken anti-GFP primary antibody (1:4000, 06-896, Millipore Bioscience) and rabbit anti-chicken secondary antibody conjugated to Alexa Fluor-488 (1:1000, 1-11039; Life Technologies). In some experiments, the position of the recording electrode was confirmed using a fluorescent DiI (Life Technologies).

GABA_BR1 immunohistochemistry was performed as described in Valley et al. (2013) with minor modifications. Live brain tissue sections were cut (300 μm), allowed to recover for 15 min in ACSF, and then quickly transfer to ice-cold 4% PFA for 30 min. Slices were then cryoprotected in 30% sucrose overnight and 12- μm -thick sections were cut using a cryostat the next day. Immunohistochemistry against GABA_BR1 was performed the same or following day. Slices were rinsed, blocked in normal goat serum for 2 h, and incubated in primary antibody (guinea pig anti-GABA_BR1, 1:3000, AB2256; Millipore Bioscience) for 48 h at 4°C. The secondary antibody (anti-guinea pig conjugated to A647, 1:1000; Life Technologies) was incubated for 2 h. Slices were then rinsed, counterstained with DAPI, mounted with Mowiol, and imaged with a confocal microscope (LSM 700; Zeiss). Quantification of the GABA_BR1 immunoreactivity was reported as the fluorescence optical density in an optical plane where GL staining was maximal using ImageJ software.

Data analysis

For light-evoked field potentials, a 10 min time window before and 10 min after drug injection was used to average evoked signals. For the fEPSP characterization, the steepest slope calculated in a 1 ms window was measured to avoid contamination by the fiber volley component. Similar results were found when measuring the slope between 20% and 80% of the descending phase of the peak. When discernable, the amplitude of the fiber volley was also measured.

For measurements of M/T cell-spiking activity, a minimal 10 min time window before and 10 min after drug injection were used for the analysis (up to 40 min before and after drug application). Signals were high-pass filtered (0.3–9 kHz) and spike detection, sorting, clustering, and spike waveform analysis were performed using Spike2 software (CED) followed by manual cluster adjustment. For single-unit validation, all sorted cells displaying >1% of their interspike intervals below a 3.5 ms refractory period were discarded from the analysis. Careful attention was taken to discard any unit that showed some significant change in spike amplitude or waveform caused by the local infusion of drugs.

We determined whether a cell receives significant inhibition or excitation by extracting individual trials and comparing the firing rate during light to the basal firing rate using a Wilcoxon matched-pairs rank-sum test. A 1 s time window was used to detect whether the cell receives significant inhibition after repeated light stimulation. A 15 ms sliding time window after light stimulation and a 5 ms sliding window, respectively, were used to detect inhibition and excitation elicited by a single light pulse.

The change in firing rate to repeated light stimulation (see Fig. 3) was calculated as follows:

M/T cell firing rate change

$$= \frac{\text{firing rate (stimulus, 1 s)} - \text{basal firing rate (1 s)}}{\text{basal firing rate (1 s)}} \times 100$$

With the firing rate (stimulus, 1 s) being the M/T cell's firing rate during the stimulation (light, odor, or both) and the basal firing rate the averaged cell's firing rate during the second before the light stimulation.

In Figure 4B, the normalized firing rate in response to a single light pulse was calculated as follows:

Normalized M/T cell firing rate (t)

$$= \frac{\text{firing rate (light, 2 ms)} - \text{basal firing rate (2 ms)}}{\text{firing rate (light, 2 ms)} + \text{basal firing rate (2 ms)}}$$

With the firing rate (light, 2 ms) being the M/T cell's firing rate over a 2 ms period during the light stimulation and the basal firing rate (2 ms) being the cell's firing rate during the 20 ms preceding light stimulation reported to a 2 ms time period.

For the analysis of direct excitation in Figure 4D, the M/T cell's firing activity was normalized as follows:

M/T cell firing rate change (t)

$$= \frac{\text{firing rate (light, 1 ms)} - \text{basal firing rate (1 ms)}}{\text{basal firing rate (1 ms)}}$$

With firing rate (light, 1 ms) being the M/T cell's firing rate over a 1 ms period during the light stimulation and basal firing rate (1 ms) being the cell's firing rate during the 20 ms preceding light stimulation reported to a 1 ms time period. To analyze the coupling between AOC stimuli and M/T cell firing (see Fig. 4E), light pulses from the same stimulation train were pooled and the same calculation as above was performed, with the firing rate (light, 10 ms) being the average number of spikes in a 10 ms time window starting 1 ms after light onset and the basal firing rate being the average number of spikes in the 10 ms time window directly preceding light stimulation.

For phase modulation analysis, the thermocouple signal was down-sampled (0.5 kHz) and filtered (0–10 Hz) to extract the sniffing signal. Oscillation peaks (exhalation end) were identified using an automatic threshold algorithm and a phase histogram (72 bins) of M/T cell spikes relative to the identified peak was computed to measure the phase preference and length of the normalized vector as a measure of modulation strength.

For spontaneous oscillations, signals were down-sampled (5 kHz) and low-pass filtered (0–300 Hz), and 10-min-long epochs excluding 1.5 s after onset of light stimulation (0.5 s after the end of the stimulation) were extracted and subjected to a fast Fourier transformation (Hanning window, 2.44 Hz resolution) to obtain the power spectrum and the spectral power in each frequency band of interest.

For photometry experiments, signals were smoothed (0.02 s window) and down-sampled to 500 Hz. For each trial, the signal was normalized to the averaged fluorescence of the trial using the $\Delta F/F$ ratio as follows:

$$\frac{\Delta F}{F}(t) = \frac{F(t) - F_0}{F_0}$$

With F_0 being the average fluorescence over the trial. Sessions with significant averaged changes in the reflected blue light ($>1\%$ $\Delta F/F$) were discarded from the analysis.

Statistics

All reported variances are SEM. In all graphs, excluding the box-and-whiskers plots, the mean is represented. In box-and-whiskers plots, the line in the middle of the box represents the median, the box edges represent the 25th to 75th percentiles and the whiskers represent the minimum and the maximum. All two-tailed Wilcoxon signed-rank tests, Mann-Whitney tests, ANOVAs, and curve fit were performed using commercial analysis software (GraphPad Prism) with $p < 0.05$ considered significant. For circular data, Hotelling paired test (significance $p < 0.05$) was performed with Oriana (Kovac Computing Services).

Results

Activation of presynaptic GABA_BRs depresses cortical synaptic transmission onto granule cells

Because AOC projections to the OB predominantly innervate the GCL (Haberly and Price, 1978a, 1978b; Davis and Macrides, 1981) and, because previous immunohistochemical studies reported the presence of GABA_BR subunits in that layer (Margeta-Mitrovic et al., 1999), we investigated the presence and the functional role of GABA_BRs at AOC-to-OB synapses. We injected the AOC of adult mice with AAV to express ChR2 in cortico-bulbar axons (Fig. 1A–C). As reported previously, ChR2-eYFP expression was confined mainly to the GCL and found to a minor extent in the mitral cell and glomerular layers (see also Haberly and Price, 1978a, 1978b; Davis and Macrides, 1981; Boyd et al., 2012; Markopoulos et al., 2012). No labeled somas were seen across bulbar layers (Fig. 1B, D) as already reported (Lepousez et al., 2014). Light stimulation of ChR2⁺ axons in horizontal OB slices (Fig. 1E) evoked monosynaptic EPSCs in voltage-clamped GCs that were abolished upon GABA_BR agonist R/S-baclofen treatment (hereafter referred as baclofen, 250 μM) and subsequent application of GABA_BR antagonist CGP-52432 (hereafter referred to as CGP, 10 μM) partially restored the EPSC amplitude ($-79.9 \pm 3.8\%$ in baclofen and $-20.2 \pm 15.2\%$ in CGP, one-way ANOVA: $p = 0.0009$, Dunn's *post hoc* test: $p < 0.05$ for baseline vs baclofen and $p < 0.01$ for baclofen vs CGP; $n = 8$; Fig. 1F). Previous slice studies showed that baclofen application did not affect GC resting membrane potential, input resistance, or threshold to spike (Isaacson and Vitten, 2003; Valley et al., 2013), suggesting no direct postsynaptic action of baclofen onto GCs. In addition to direct excitatory inputs, cortico-bulbar axons light stimulation produced disynaptic inhibition onto GCs, presumably originating from deep short axon cells (Boyd et al., 2012; Markopoulos et al., 2012). NBQX-sensitive IPSCs were recorded in 8 of the 35 recorded GCs and these IPSCs were blocked by baclofen and restored with CGP application ($-80.1 \pm 4.3\%$ in baclofen, $-20.1 \pm 9.7\%$ in CGP and $-89.5 \pm 2.4\%$; in NBQX, one-way ANOVA: $p = 0.0005$, $p < 0.01$ for baseline vs baclofen and $p < 0.05$ for baseline vs NBQX and baclofen vs CGP; $n = 7$; Fig. 1G).

We next evaluated the *in vivo* functional impact of GABA_BR modulation on the OB circuit activity. We recorded LFP *in vivo* and induced light stimulation of ChR2⁺ axon terminals with an optic fiber positioned at the OB surface (Fig. 2A). A field response composed of an early (N1) and late (N2) component was observed (Fig. 2B, C). Although the voltage depth profile of N1 (peaking at ~ 2 ms) was monotonic across OB layers, N2 reversed polarity at the mitral cell layer (Fig. 2B), indicating that N2 encompassed a current sink in the GCL and a current source in the EPL, as reported in studies using electrical stimulation in the APC (Neville and Haberly, 2003; Manabe et al., 2011). These signals were generated mainly by GC depolarization because these cells and their dendrites occupy the vast majority of the space in the GCL and in the EPL and are morphologically organized as a dipole between these two layers (Rall and Shepherd, 1968). Pharmacological characterization in anesthetized animals showed that local microinfusion of AMPA receptor antagonist NBQX (1 mM) into the GCL strongly reduced the N2 slope, with no significant effect on the N1 amplitude (N2: $-69.5 \pm 10.9\%$; N1: $-8.9 \pm 4.9\%$, $n = 3$; Fig. 2C). In contrast, local infusion of lidocaine (2%), a voltage-gated Na⁺ channel blocker, strongly decreased both N1 and N2 (N2: $-60.4 \pm 1.7\%$; N1: $-79.8 \pm 5.9\%$, $n = 4$; Fig. 2C; two-way ANOVA: drug effect: $F_{(2,19)} = 54.6$,

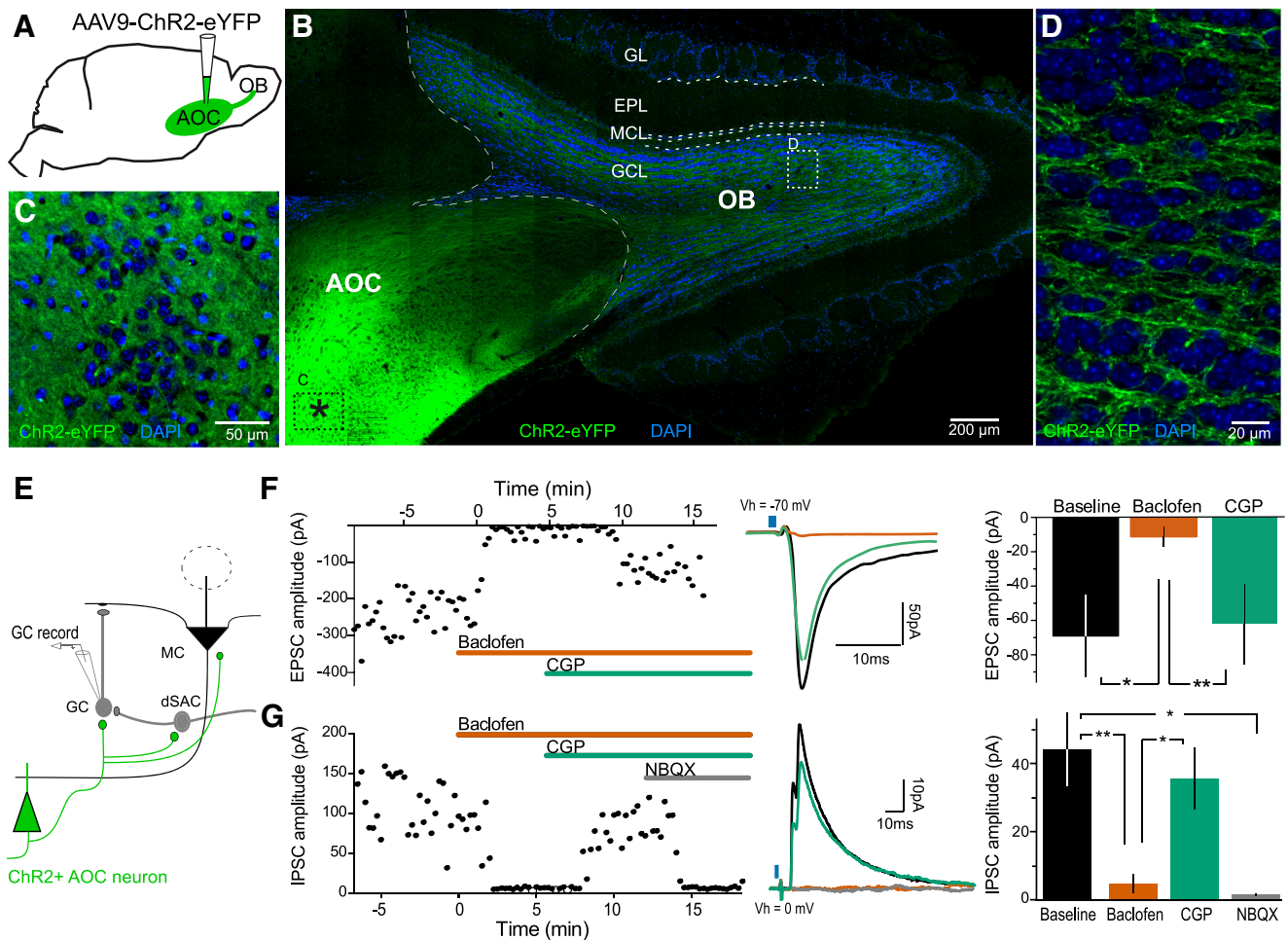


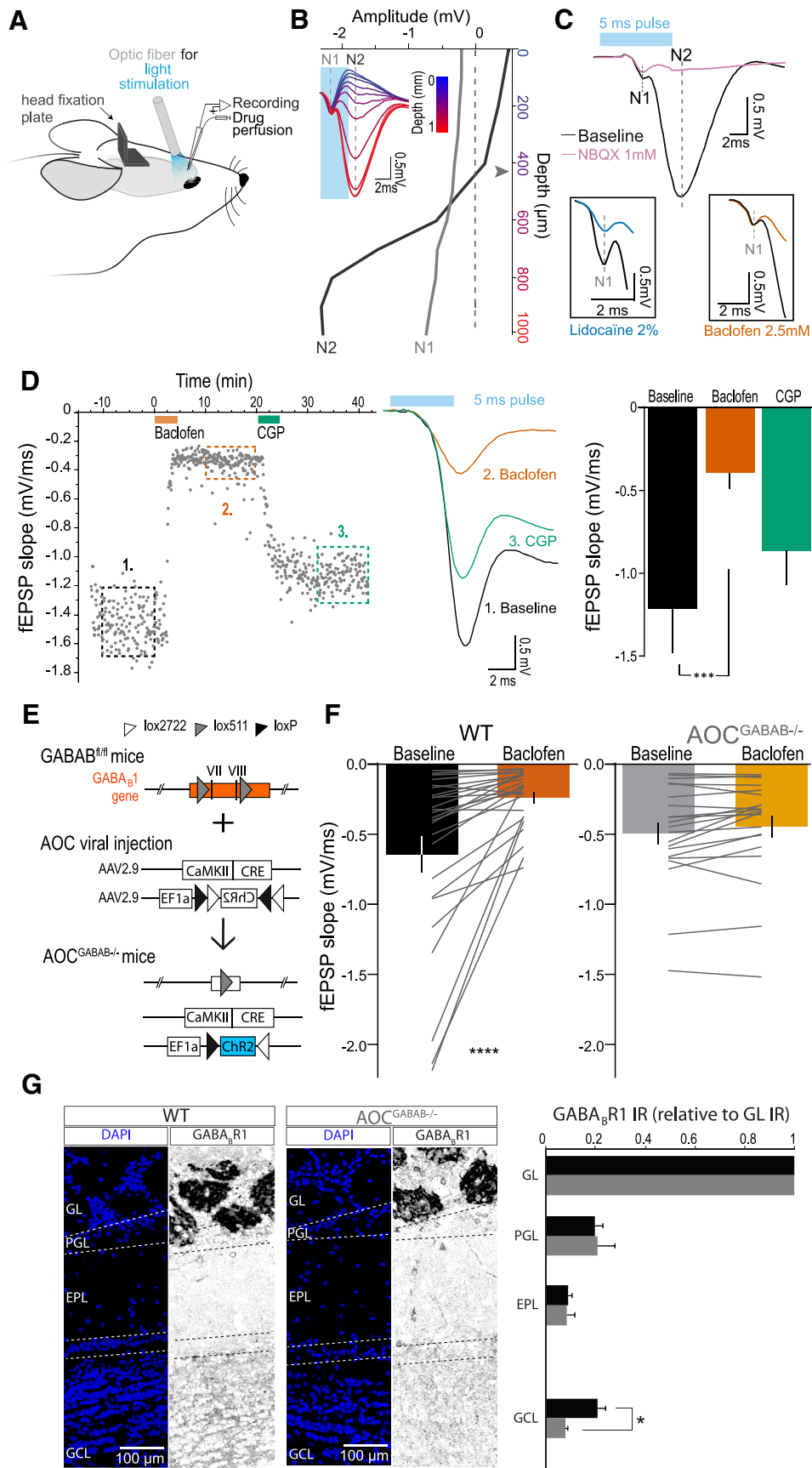
Figure 1. GABA_B activation depresses the glutamatergic AOC-to-GC synapse *in vitro*. **A**, Schematic representing AAV2/9-ChR2-eYFP injection into the AOC and cortico-bulbar ChR2⁺ axons targeting the OB. **B**, Horizontal section showing the injection site (*) in the AOC and ChR2 expression along the OB layers. ChR2-eYFP expression was mainly confined to the GCL. **C**, Higher magnification of region “C” in **B** indicating ChR2 expression in the AOC. **D**, Higher magnification of region “D” in **B** showing the dense ChR2-eYFP expression in the OB GCL and the absence of ChR2⁺ soma. **E**, Recording schematic. GCs were patched and cortico-bulbar axons were light stimulated. **F**, AOC axon light stimulation evoked GABA_B-sensitive excitation in GCs. Left, EPSC amplitude time course in basal, baclofen (250 μM), and CGP 52432 (10 μM) conditions. Middle, Representative averaged traces. Right, Averaged EPSC amplitudes. **G**, AOC axon light stimulation evoked GABA_B-sensitive disinhibition in GCs. Left, IPSC amplitude time course in basal, baclofen (250 μM), CGP 52432 (10 μM), and NBQX (10 μM) conditions. Middle, Representative averaged traces. Right, Average IPSC amplitudes. GL, Glomerular layer; EPL, external plexiform layer; MCL, mitral cell layer; GCL, granule cell layer. MC, mitral cell; GC, granule cell; dSAC, deep short axon cell. **p* < 0.05, ***p* < 0.01 with a Dunn’s multiple-comparisons test after one-way ANOVA.

p < 0.0001 and drug × negativity: $F_{(2,19)} = 6.8$, *p* = 0.006, Holm–Sidak’s multiple-comparisons *post hoc* test: N1: *p* = 0.48 for NBQX and *p* < 0.0001 for lidocaine, N2: *p* < 0.0001 for both drugs compared with vehicle); vehicle injection had no effect on N1 or N2 (*p* = 0.32, *n* = 4; *p* = 0.94, *n* = 7; respectively). Both N1 and N2 amplitude increased with the power of photostimulation and disappeared in the absence of ChR2. Together with recent studies reporting that light stimulation of cortico-bulbar axon terminals drives direct excitation of GCs (Boyd et al., 2012; Markopoulos et al., 2012), our data strongly suggest that N1 is a ChR2⁺-induced Na⁺-spike-dependent fiber volley invading AOC axon terminals, while N2 is a fEPSP generated by AMPAR-dependent depolarization, specific to GCs.

In anesthetized and awake head-restrained mice, local micro-infusion of baclofen (2.5 mM) in the GCL did not alter the fiber volley ($-3.2 \pm 2.7\%$, *n* = 4, Wilcoxon matched-pairs signed-rank test: *p* = 0.63; Fig. 2C), but produced a 2-fold decrease in amplitude and slope of the light-evoked fEPSP. This effect was reversed by subsequent application of CGP (100 μM; fEPSP slope: $-65.5 \pm 8.6\%$ in baclofen and $-32.5 \pm 8.5\%$ in CGP; fEPSP

amplitude: $-56.18 \pm 7.3\%$ in baclofen and $-20.0 \pm 11.5\%$ in CGP; one-way ANOVA: *p* < 0.0003 for both slope and amplitude, Dunn’s multiple-comparisons *post hoc* test: baseline vs baclofen: *p* < 0.001 for slope and amplitude, baclofen vs CGP *p* < 0.05 for amplitude and *p* = 0.074 for slope; *n* = 8; Fig. 2D).

To estimate the diffusion of baclofen in the OB, we first validated that, after a first baclofen injection, the second injection at the same site did not depress further the fEPSP amplitude and slope, which is compatible with local saturation of GABA_BRs. However when baclofen was injected a second time ~500–600 μm below we observed a strong reduction of the fEPSP, comparable to the reduction observed after the first dorsal injection ($-63.3 \pm 7.8\%$, *p* = 0.23 with Wilcoxon signed-rank test, *n* = 5). This suggests that the first injection did not reach the second site located ~500–600 μm deeper in the GCL. To confirm this observation, we injected the same volume and concentration of the nuclear dye DAPI and *post hoc* histological analysis permitted us to estimate the dye diffusion to be <500 μm. We concluded that, using our injection protocol, baclofen cannot diffuse in an area >600 μm within the OB and therefore cannot significantly dif-



fuse to the AOC. Furthermore, we did not observe any significant difference between anesthetized and awake mice in the structure of the light-evoked fEPSP or in the effect of baclofen ($-48.5 \pm 4.5\%$ in anesthetized vs $-47.0 \pm 5.7\%$ in awake mice, $n = 8$ and 25 , respectively, $p = 0.98$), and data were therefore pooled. However, because cortico-bulbar top-down inputs are sensitive to wakefulness (Boyd et al., 2015; Otazu et al., 2015), the ensuing *in vivo* experiments were performed solely in awake animals.

To strengthen our *in vitro* results suggesting a presynaptic localization of GABA_BRs at the AOC-to-GC synapse (Fig. 1F), we designed a conditional knock-out approach to delete GABA_BRs in a region-specific manner. A transgenic mouse line that possesses critical exons VII and VIII of the GABA_B(1) gene flanked with lox sites (GABAB^{fl/fl} mice; Haller et al., 2004) was used. To knock-out the expression of GABA_BRs and express Chr2 in the same population of cortico-bulbar fibers, two AAVs expressing either Cre recombinase (AAV-CaMKIIa-Cre) and a Cre-dependent Chr2 (AAV-EF1a-DIO-Chr2-mCherry) were co-injected in the AOC of age-matched WT ($n = 5$) and GABAB^{fl/fl} mice ($n = 4$). Using this strategy, Chr2-eYFP was a reporter for Cre expression and thus identified the population of cells in which GABA_BRs were conditionally knocked out in GABAB^{fl/fl} mice (hereafter named AOC^{GABAB^{-/-}}) (Fig. 2E). As a control, we injected AAV directly expressing Chr2 under the control of the CaMKIIa promoter in WT mice (AAV-CaMKIIa-Chr2-EYFP; $n = 7$). Three months after viral injection, Cre expression led to Chr2-mCherry labeling of cortico-bulbar axons. In awake animals, baclofen caused a 2-fold decrease in the light-evoked fEPSP slope and amplitude in WT mice, but had no significant effect in AOC^{GABAB^{-/-}} mice (WT: slope: $-49.4 \pm 6.1\%$, amplitude: $-47.0 \pm 5.6\%$, $n = 25$ and AOC^{GABAB^{-/-}}: slope: $-6.3 \pm 5\%$, amplitude: $-7.3 \pm 3.2\%$, $n = 21$; Two-way ANOVA on slope: baclofen \times genotype: $F_{(1,44)} = 9.26$, $p = 0.004$; Fisher's *post hoc* test: $p < 0.0001$ in WT animals and $p = 0.57$ in AOC^{GABAB^{-/-}} mice; on amplitude: $F_{(1,44)} = 9.37$, $p = 0.004$; Fisher's *post hoc* test: $p < 0.0001$ in WT and $p = 0.58$ in AOC^{GABAB^{-/-}}; saline in WT: $-4.8 \pm 7.5\%$, $n = 7$, Wilcoxon matched-pairs signed-rank test: $p = 0.94$; Fig. 2F). To confirm that GABA_BR expression was indeed diminished in cortico-bulbar axons, we performed immunohistochemical labeling for the GABA_BR1 subunit in OB slices. The immunoreactivity was decreased selectively in the

GCL of AOC^{GABAB^{-/-}} mice, but not in the GCL of WT animals (interaction genotype \times OB layer: $F_{(2,14)} = 4.41$, $p = 0.033$, $p = 0.049$ for the GCL and $p > 0.05$ for the other layers, $n = 5$ WT and $n = 4$ AOC^{GABAB^{-/-}}; Fig. 2G). Together, these data demonstrate that the expression of presynaptic GABA_BRs in cortico-bulbar axons allows depression of excitatory feedback onto GCs.

Activation of presynaptic GABA_BRs depresses cortico-bulbar feedforward inhibition onto M/T cells

We next examined the effect of GABA_BR activation in cortical fibers on M/T cell spontaneous firing activity. Extracellular recordings of M/T cells (see Materials and Methods section for identification criteria) were performed in awake, head-restrained mice and the same cells were recorded before and after local perfusion of baclofen within the vicinity of the electrode (Fig. 3A). In WT and AOC^{GABAB^{-/-}} mice, baclofen did not alter the M/T cell spontaneous firing rate ($-8.3 \pm 4.0\%$ in WT, $n = 42$; $-0.3 \pm 4.5\%$ in AOC^{GABAB^{-/-}}, $n = 29$; two-way ANOVA: $F_{(1,69)} = 2.75$, $p = 0.10$), consistent with an *in vitro* study reporting no postsynaptic effect of baclofen on M/T cells (Isaacson and Vitten, 2003). We also investigated whether baclofen changes the temporal relationship between M/T cell firing and the sniff cycle. At the population level, M/T cell phase preference to the sniff cycle did not significantly shift with baclofen application ($+40.8 \pm 34.7^\circ$ in WT, $n = 17$, and $-28.9 \pm 45.4^\circ$ in AOC^{GABAB^{-/-}} animals, $n = 16$, $p = 0.33$ and $p = 0.15$ with a paired Hotelling test), whereas it induced a small increase in the strength of the sniffing modulation of M/T cell firing activity in WT, but not AOC^{GABAB^{-/-}} mice (mean vector length: baseline: 0.07 ± 0.01 ; baclofen: 0.11 ± 0.01 ; baclofen: $F_{(1,39)} = 5.93$, $p = 0.02$; however, baclofen \times genotype interaction: $F_{(1,39)} = 3.64$, $p = 0.064$; Fisher's LSD *post hoc* test: WT: $p = 0.0013$, $n = 25$, AOC^{GABAB^{-/-}}: $p = 0.74$, $n = 16$).

Previous OB slice experiments showed that cortico-bulbar stimulation drives disynaptic inhibition onto M/T cells, mainly mediated by GCs, which is abolished by glutamatergic blockers (Balu et al., 2007; Boyd et al., 2012; Markopoulos et al., 2012). Here, we applied a 1 s light train stimulation on cortico-bulbar axons while recording M/T cell activity using an optic fiber positioned either on top of the OB surface or implanted above the anterior commissure. Because the olfactory cortex send back information to the OB at various regimes (beta, 15–40 Hz, by Gray and Skinner, 1988; Neville and Haberly, 2003; Martin et al., 2006; gamma frequencies, 40–100 Hz, by Boyd et al., 2012; theta, 1–10 Hz, by Youngstrom and Strowbridge, 2015), we decided to span the whole spectrum of cortical axon activity with stimulation frequencies ranging from 10 to 100 Hz. Figure 3B shows the response of an example M/T cell to three frequencies of light stimulation (10, 33, and 67 Hz) and Figure 3C illustrates the inhibition triggered by the different light stimulation patterns on each individual recorded M/T cells. The percentage of change in firing rate is color coded (blue represents inhibition and red excitation). 21/22 of the recorded M/T cells ($\sim 95\%$) showed reduced firing activity upon cortical stimulation (Wilcoxon matched-pairs rank-sum test for each cell, light stimulation vs prestimulation, $p < 0.05$; Fig. 3C, left), as reported previously (Markopoulos et al., 2012; Soria-Gómez et al., 2014). The percentage of inhibition was not related to the cell's spontaneous firing rate ($y = 0.0041x - 0.73$, $R^2 = 0.012$, slope not different from 0: $p = 0.63$, $n = 21$), and maximum inhibition was distributed from 33 to 50 Hz (Fig. 3D). Figure 3E represents the effect of 33 Hz light stimulation on individual M/T cells. At the M/T cell population level, firing inhibition as a function of stimulation

←

Figure 2. Presynaptic GABA_BR activation depresses the glutamatergic AOC-to-GC synapse *in vivo*. **A**, Schematic drawing of the recording configuration. In head-restrained mice, Chr2⁺ axons were optogenetically stimulated by delivering light through an optic fiber. Drugs were perfused using a miniature cannula in the vicinity of the electrode tips. **B**, Light-evoked field recordings across the different OB layers (color-coded, inset). Depth profile of events N1 and N2 is reported. Arrowhead indicates the depth at which N2 reversed polarity. **C**, Pharmacological characterization of N1 and N2. N1 was depressed by 2% lidocaine but remained unaffected by NBQX (1 mM), baclofen (2.5 mM), or vehicle application. N2 was decreased by lidocaine and NBQX, but not vehicle. **D**, Light-evoked fEPSP was modulated by GABA_BR. Left, fEPSP slope time course in basal, baclofen (25 mM), and CGP 52432 (100 μM) condition. Middle, Representative averaged traces. Right, Average fEPSP slope. **E**, Schematic of the conditional knock-out approach. In GABAB^{fl/fl} mice, co-injection of AAV2/9-CaMKII-Cre and AAV2/9-EF1a-DIO-Chr2 viruses in the AOC led to a nonfunctional GABA_BR1 gene in the neuronal population excitable with light. **F**, Baclofen depressed the fEPSP slope in WT, but not in AOC^{GABAB^{-/-}} mice. **G**, Immunohistochemical staining against GABA_BR1. Left, Horizontal OB sections showing the distribution of GABA_BR1 expression across the layers in a WT and a AOC^{GABAB^{-/-}} mouse (inverted grayscale). Quantifications (right; GL immunoreactivity set to 1) revealed a specific reduction of GABA_BR1 immunoreactivity in the GCL of AOC^{GABAB^{-/-}} mice. PGL, periglomerular layer. *** $p < 0.001$ with a Dunn's multiple-comparisons test after one-way ANOVA * $p < 0.05$, **** $p < 0.0001$ with a Fisher's LSD test after two-way ANOVA.

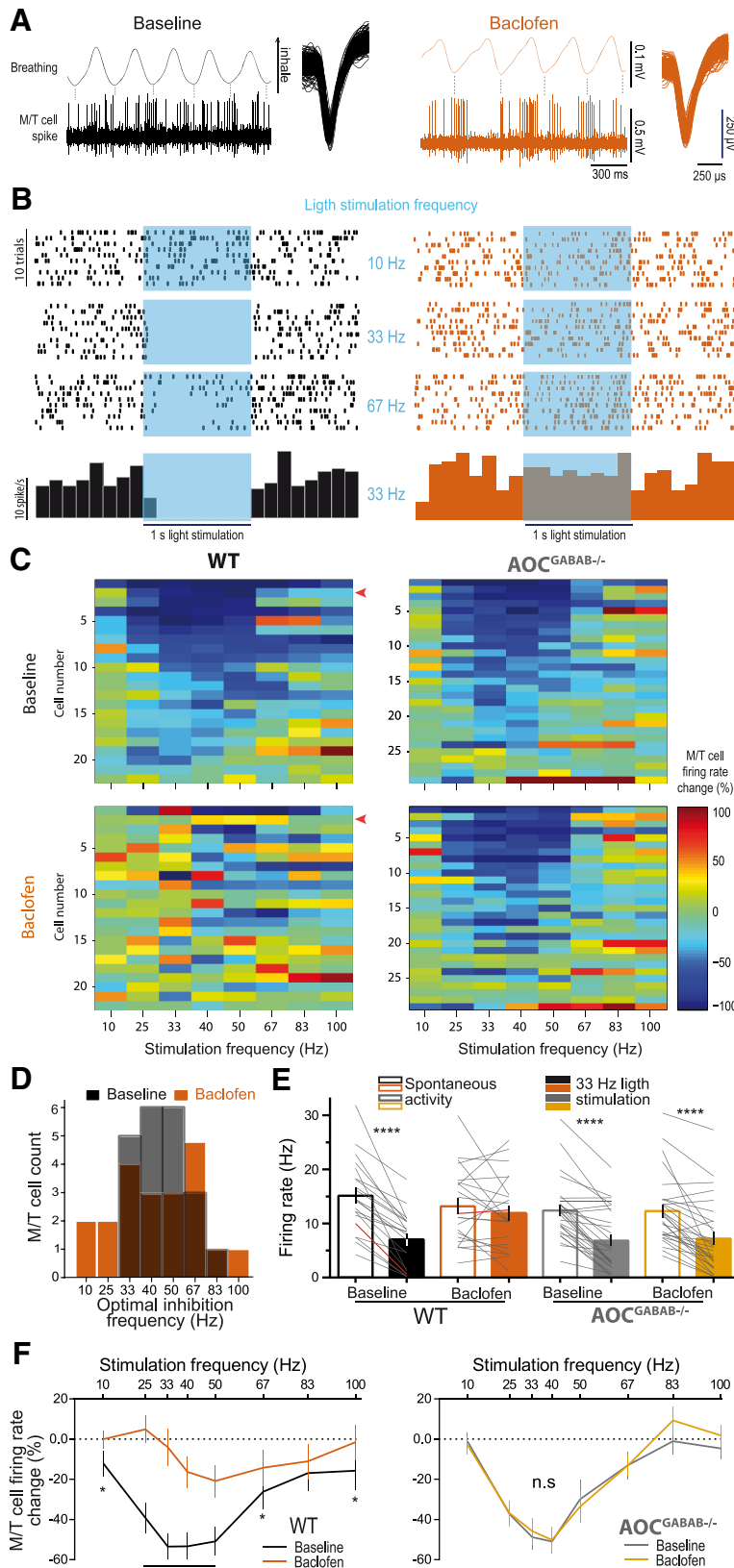


Figure 3. GABA_BR activation at AOC axon terminals suppresses inhibition onto M/T cells. **A**, Example of M/T cell awake spontaneous spiking activity associated with breathing signal during basal and baclofen (2.5 mM) conditions. **B**, Top, Raster plot of a cell's response to patterned light stimulation (10, 33 and 100 Hz, 1 s) of AOC axons before (left) and after baclofen application (right). Bottom, PSTH of the neuron's response to 40 Hz light stimulation. **C**, Heat map of individual neuron's response in WT ($n = 22$, left) and AOC^{GABAB-/-} mice ($n = 29$, right) to the different light stimulation frequencies in baseline (top) and baclofen

frequency followed a bell-shaped curve with 33–50 Hz driving maximum inhibition (from $-13.0 \pm 6.7\%$ at 10 Hz to $-55.9 \pm 6.4\%$ at 33 Hz; $n = 21$ cells; Fig. 3F, left). When the same cells were recorded in the presence of baclofen, the magnitude of the light-evoked inhibition of M/T cells decreased significantly. For example, the powerful inhibition induced by 33 Hz light delivery in baseline conditions was abolished in presence of baclofen ($-53.2 \pm 6.8\%$ in basal condition and $-1.3 \pm 12\%$ in baclofen; baclofen: $F_{(1,20)} = 24.92$, $p < 0.0001$; baclofen \times light interaction: $F_{(1,20)} = 20.31$, $p = 0.0002$, Fisher's LSD *post hoc* test: $p < 0.0001$ in basal condition and $p = 0.23$ in baclofen; Figure 3E). CGP application partially restored the light-induced inhibition (e.g., M/T cell firing change at 33 Hz: $-92.4 \pm 4.7\%$ in baseline, $-8.0 \pm 20.1\%$ in baclofen and $-47.0 \pm 12.3\%$ in CGP, $n = 2$). Across all frequencies, baclofen blocked the light-induced inhibition of M/T cells (baclofen and baclofen \times light frequency interaction: $F_{(1,21)} = 20.31$, $p = 0.0002$ and $F_{(7,147)} = 8.41$, $p < 0.0001$, respectively; Fisher's LSD *post hoc* test, $p < 0.05$ except for 83 Hz light stimulation, where $p = 0.31$, $n = 21$; Fig. 3C,F), whereas vehicle application had no effect ($F_{(1,7)} = 0.80$, $p = 0.40$, $n = 8$).

Because M/T cell inhibition could also be blocked by GABA_BR action at the GC dendrodendritic synapse (Isaacson and Vitten, 2003; Valley et al., 2013), the same experiments were performed in AOC^{GABAB-/-} mice. In these transgenic animals, light stimulation delivered at various frequencies decreased M/T cell firing with a similar bell-shaped relationship ($n = 29$ cells; Fig. 3F, right) and individual M/T cells displayed light-evoked inhibition comparable to WT mice (e.g., for 33 Hz stimulation: $-48.8 \pm 6.1\%$ in M/T cell firing rate, $n = 29$ cells; Fig. 3C,E). However, baclofen did not alter the light-evoked inhibition of M/T cell in

(bottom) conditions. Blue represents inhibition and red excitation. Red arrow indicates the example cell in **B**. **D**, Distribution of the frequencies driving maximum inhibition across M/T cell population. **E**, Effect of 33 Hz light stimulation on individual M/T cell firing rate before and after baclofen application in WT and AOC^{GABAB-/-} animals. Red lines represent the example cell shown in **B**. Note that baclofen did not affect the M/T cell spontaneous firing rate. **F**, Percentage of firing rate change before and after baclofen application as a function of stimulation frequency. AOC axon stimulation produces a similar tuning curve to light frequencies in WT and AOC^{GABAB-/-} mice. * $p < 0.05$, **** $p < 0.0001$ with a Fisher's LSD test after two-way ANOVA.

these animals ($F_{(1,28)} = 0.46, p = 0.50, n = 29$; Fig. 3C,F). Therefore, these results demonstrate that presynaptic GABA_BR activation at cortico-bulbar axon terminals blocks M/T cell feedforward inhibition.

During these experiments, the influence of cortical inputs on the OB activity was revealed using long-lasting and repeated light stimulation. To examine M/T cell responses to transiently active AOC inputs, we analyzed M/T cell firing activity in response to a single, 5-ms-brief light pulse. In WT mice, 18/22 M/T cells (~82%) showed a transient suppression of their firing after such a brief light stimulation (Wilcoxon matched-pairs rank-sum test for each cell, $p < 0.05$). Figure 4A shows a representative cell responding to a single 5 ms light pulse before and after baclofen treatment (top and bottom, respectively). This rapid, transient inhibition of M/T cell firing peaked at 10 ms and lasted ~30 ms (Fig. 4A,B). Baclofen treatment decreased this inhibition (two-way ANOVA: $F_{(1,17)} = 12.39, p = 0.003$; baclofen \times time interaction, $F_{(34,578)} = 9.55, p < 0.0001$, Sidak's multiple-comparisons test: $0.0001 < p < 0.05$ between 4 and 14 ms after light onset; $n = 18$; Fig. 4A,B) and dampened the peak amplitude ($-20.7 \pm 8.1\%$ in baclofen; Wilcoxon match-pairs rank-sum test: $p = 0.009, n = 18$), resulting in only 13 of 22 recorded cells still showing significant inhibition after baclofen treatment. This feedforward inhibition decayed with a time constant of 17.3 ms in basal conditions and 20.9 ms with baclofen application ($r^2 = 0.96$ and 0.65 , respectively; not significantly different, $p = 0.29, n = 18$) and recovered after CGP infusion ($n = 2$). In AOC^{GABAB^{-/-}} animals, the light-evoked inhibition was observed in all M/T cells recorded under basal conditions (29/29) and in 28 of 29 recorded cells with baclofen treatment. Baclofen application did not change the time course of inhibition ($F_{(1,28)} = 0.612, p = 0.44, n = 29$) or the peak amplitude ($-2.4 \pm 4.3\%, p = 0.49, n = 29$) (Fig. 4B). These results demonstrate that brief light stimulation of AOC axons is sufficient to elicit feedforward inhibition onto M/T cells and GABA_BR activation can depress this disinaptic inhibition driven by single cortical inputs.

Cortical feedback excitation to M/T cells is insensitive to presynaptic GABA_BR modulation

Because AOC glutamatergic afferents to the OB also excite M/T cells directly (Markopoulos et al., 2012; Fig. 1E), we next examined direct excitation from AOC axons in the same M/T cell population. Figure 4C shows an example M/T cell responding with a rapid and precise increase of firing activity in response to a single 5-ms-long light pulse in both basal and baclofen conditions. We found that 7/22 (~32%) of M/T cell cells received significant direct excitatory input in basal conditions (Wilcoxon match-pairs rank-sum test for each cell). In the 7 M/T cells exhibiting direct excitation before and after baclofen treatment, we observed a slightly prolonged excitation in baclofen conditions, although not significant (two-way ANOVA: interaction time \times baclofen: $F_{(29,174)} = 1.01, p = 0.46$; baclofen: $F_{(1,6)} = 5.12, p = 0.064; n = 7$; Fig. 4D). No difference was observed in the peak amplitude or in the latency to peak (peak amplitude: $+4.6 \pm 4.3\%$ in baclofen, $p > 0.99$; peak latency: 3.0 ± 0.6 ms in baseline vs 2.9 ± 0.5 ms in baclofen, $p > 0.99$, Wilcoxon match-pairs tests; $n = 7$; Fig. 4D). We also observed that 2/14 cells showed direct excitation with baclofen treatment, but not in basal conditions. In AOC^{GABAB^{-/-}} mice, we detected a significant direct excitation in 17/29 (~59%) of the recorded M/T cells. After baclofen administration, 20/29 (~70%) M/T cells received significant excitation, but baclofen treatment had no effect on this excitation (time \times baclofen interaction: $F_{(29,464)} = 0.73, p = 0.85$; peak

amplitude: $-11.4 \pm 15.9\%$ in baclofen, $p = 0.0984$; and peak latency: 4.35 ± 0.56 ms in baseline and 4.59 ± 0.54 ms in baclofen, $p = 0.47; n = 17$; Fig. 4D).

In vitro, light activation of AOC axons failed to reveal fast excitatory synaptic responses on M/T cells, which would have supported the fast evoked firing activity observed *in vivo*. Instead, we observed small, slow inward currents (average amplitude -9.3 ± 0.9 pA, $V_h = -70$ mV; $n = 9$) blocked by NBQX ($-89.5 \pm 2.4\%; p = 0.0003; n = 6$), as described previously (Boyd et al., 2012; Markopoulos et al., 2012). Moreover, these evoked currents were frequent *in vitro* (18/24) and were blocked by baclofen ($-78.5 \pm 3.1\%$ in baclofen and $-23.8 \pm 6.7\%$ in CGP; $F_{(1,356,10,85)} = 36.31, p < 0.0001$, one-way ANOVA, $p < 0.05$ for all Holm–Sidak's *post hoc* test; $n = 9$). Conversely, light-triggered M/T cell spiking *in vivo* was rare (7/22) and insensitive to baclofen (Fig. 4D). Furthermore, the slow kinetics of the *in vitro* EPSCs (time to peak from light onset: 5.4 ± 0.5 ms) are incompatible with the *in vivo* sharp light-evoked spiking (time to peak from light onset: 3.0 ± 0.6 ms). In addition, these slow EPSCs were shown to be unable to trigger M/T cell spiking in slices (Boyd et al., 2012). Collectively, these discrepant observations suggest that these slow currents recorded *in vitro* do not underlie the fast spiking that we observed *in vivo*. The recorded EPSCs *in vitro* could reflect glutamate receptor activation in electrophysiologically remote regions of M/T cell lateral dendrites or gap junctionally coupling with cells receiving direct synaptic inputs.

In vivo, because the efficiency of cortical inhibition of M/T cells is dependent on the stimulation frequency (Fig. 3F), we investigated whether GABA_BR differentially influenced M/T cell excitatory/inhibitory biphasic response driven at different frequencies. In baseline conditions, M/T cell spiking activity after cortical stimulation decreased at frequencies >10 Hz (Fig. 4E). Baclofen extended the increase in spiking activity after cortical stimulation to higher frequencies (up to 50 Hz) in WT, but not in AOC^{GABAB^{-/-}} animals (WT: frequency \times baclofen: $F_{(7,42)} = 5.87, p < 0.0001$, Fisher's *post hoc* test: $p < 0.01$ for 10 to 50 Hz; $n = 7$; AOC^{GABAB^{-/-}}: $F_{(7,91)} = 0.68, p = 0.69; n = 14$; Fig. 4E). This result indicates that GABA_BR activation extends the functional coupling between cortical excitation and M/T cells response in the 10–50 Hz activity band. In summary, activation of cortical feedback triggers both fast direct excitation and feedforward inhibition onto M/T cells, but GABA_BR activation selectively depresses the inhibitory tone while sparing excitation, thereby reformatting the ratio between excitation and feedforward inhibition received by M/T cells.

Activation of presynaptic GABA_BRs modulates OB oscillatory activity

Previous studies showed that oscillations and temporal activity might be under the control of extrinsic top-down inputs (Engel et al., 2001). Oscillatory rhythms are prominent in the OB of awake mice (Fig. 5A,B). On the top of breathing-related theta oscillations (1–10 Hz), which are largely driven by olfactory sensory inputs, gamma oscillations (40–100 Hz) are generated by the dendrodendritic synapse (Rall and Shepherd, 1968; Gray and Skinner, 1988; Neville and Haberly, 2003; Kay et al., 2009; Lepousez and Lledo, 2013), whereas beta oscillations (15–40 Hz) are thought to be driven by interactions between the olfactory cortex and the OB (Gray and Skinner, 1988; Neville and Haberly, 2003; Martin et al., 2006). In light of this circuit segregation, we sought to determine whether GABA_BR-mediated depression of AOC inputs to the OB would alter specific oscillatory frequencies. We found no change in theta power in presence of baclofen in WT or

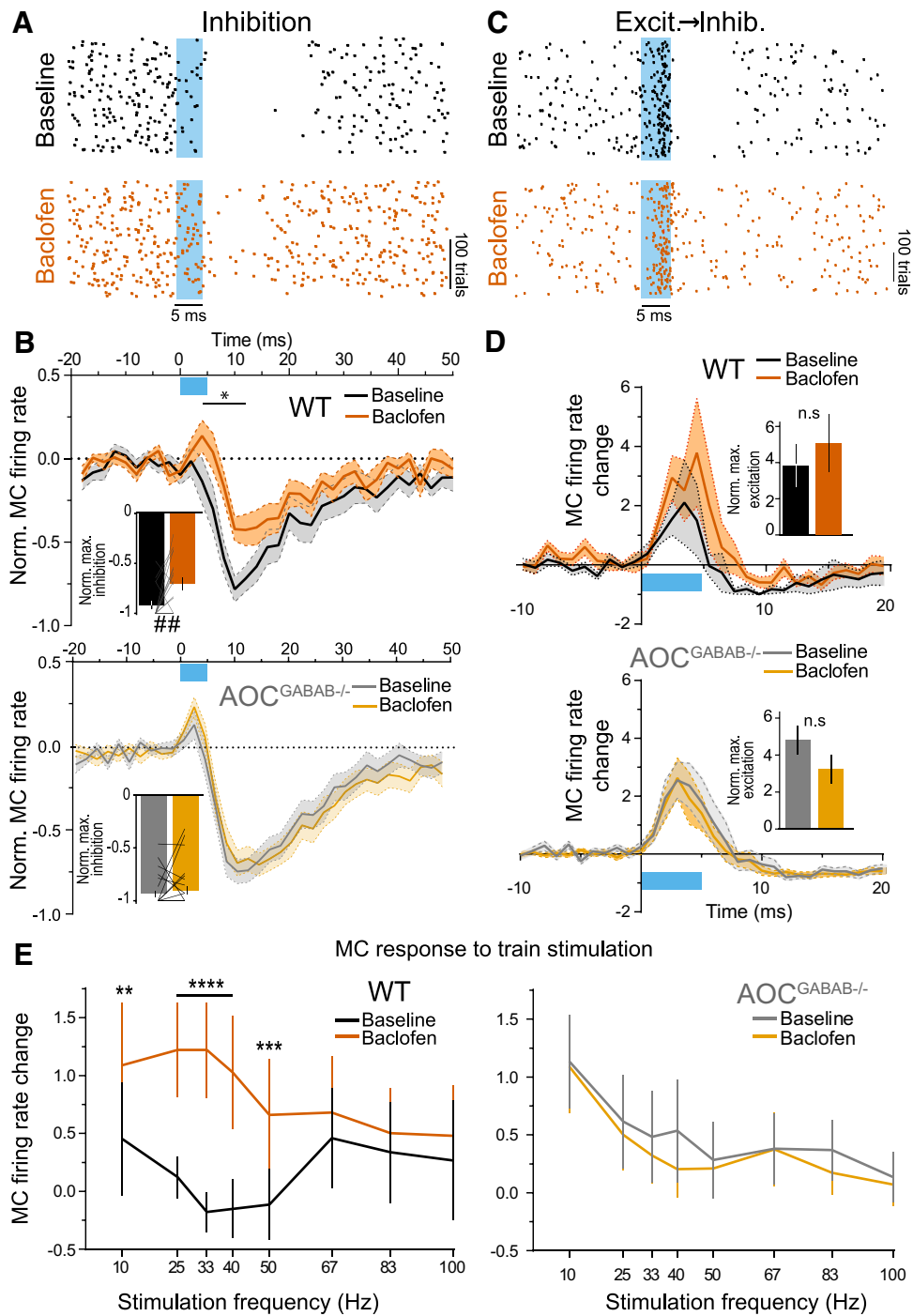


Figure 4. Single light pulse analysis reveals target-specific GABA_B modulation of cortical inputs to the OB. **A**, Raster plot of a cell inhibited by a single light pulse (5 ms), before (top) and after (bottom) baclofen (2.5 mM) application. **B**, Normalized PSTH of M/T cell population after a single light pulse delivery in WT (top), $n = 18$ and AOC^{GABAB^{-/-}} mice (bottom, $n = 29$) before and after baclofen application. Inset, Normalized firing rate trough in basal and baclofen conditions. **C**, Raster plot of a cell displaying a brief excitation followed by a prolonged inhibitory response after light stimulation and before (top) and after (bottom) baclofen application. **D**, Normalized PSTH of the M/T cell receiving direct excitation to a single light pulse in WT (top, $n = 7$) and AOC^{GABAB^{-/-}} animals (bottom, $n = 14$) before and after baclofen application. Inset, Normalized firing rate peak. **E**, M/T cell mixed excitatory/inhibitory response to AOC train light stimulation. Normalized change in M/T cell firing rate during 10 ms after light stimulation for the same neurons as in **D**. In baclofen conditions, WT M/T cell displayed a higher excitatory response to light at 10–50 Hz stimulation. $\#\#p < 0.05$ with a Wilcoxon matched-pairs rank-sum test; $*p < 0.05$ to $p < 0.0001$ with a Sidak's multiple-comparisons test after two-way ANOVA, $**p < 0.01$, $***p < 0.001$, $****p < 0.0001$ with a Fisher's LSD test after two-way ANOVA.

in AOC^{GABAB^{-/-}} animals (WT: $-0.8 \pm 15.4\%$, $n = 21$; AOC^{GABAB^{-/-}}: $-17.6 \pm 7.0\%$, $n = 29$; Two-way ANOVA, $F_{(1,48)} = 5.59$, $p < 0.02$, but Fisher's LSD *post hoc* test: $p = 0.11$ and 0.09 in WT and AOC^{GABAB^{-/-}} animals, respectively; vehicle injection in WT: $p = 0.55$, Wilcoxon matched-pairs rank-sum test, $n = 9$; Fig. 5B,C). Together with the absence of a significant

effect of baclofen on M/T cell spontaneous activity, these results suggest that local baclofen application in the GCL did not permit baclofen diffusion superficially to the GL. In contrast, baclofen strongly decreased gamma oscillations in a similar fashion in WT and AOC^{GABAB^{-/-}} animals (WT: $-42.8 \pm 5.6\%$, $n = 21$ and AOC^{GABAB^{-/-}}: $-44.0 \pm 4.3\%$, $n = 29$, $F_{(1,48)} = 20.18$, $p <$

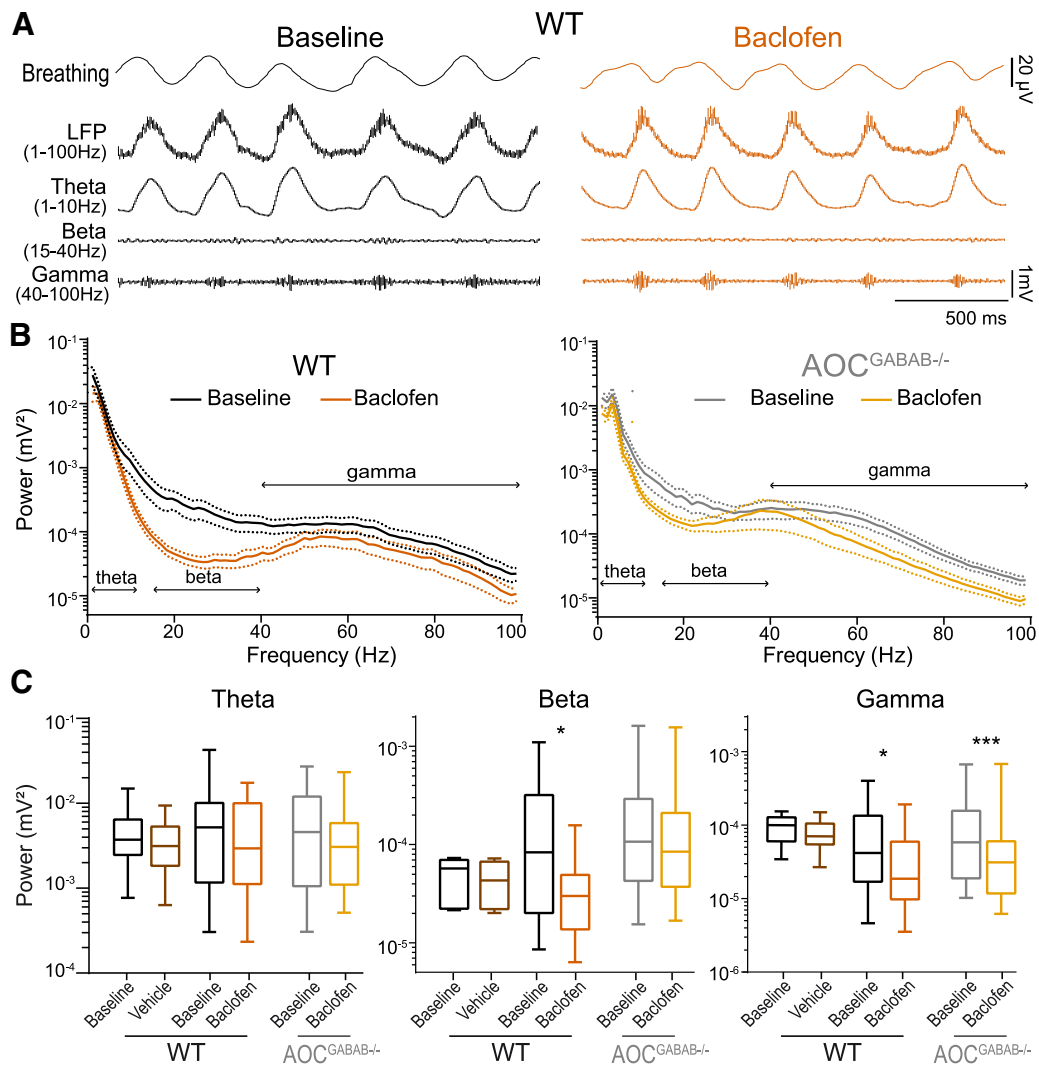


Figure 5. Activation of GABA_BRs on cortical feedback projections depresses beta OB oscillations. **A**, Example recordings of awake LFP and filtered signals showing spontaneous theta (1–10 Hz), beta (20–40), and gamma (40–100 Hz) band before (left) and after (right) baclofen (2.5 mM) injection. **B**, Whole power spectrum of spontaneous LFP before and after baclofen application in WT (left) and AOC^{GABAB-/-} (right) mice. **C**, Spontaneous theta, beta, and gamma oscillation power before and after baclofen application in WT and AOC^{GABAB-/-} animals. * $p < 0.05$, *** $p < 0.001$ with a Fisher's LSD test after two-way ANOVA.

0.0001; Fisher's LSD *post hoc* test: $p = 0.017$ in WT and $p = 0.0002$ in AOC^{GABAB-/-}, vehicle in WT: $-12.2 \pm 10.4\%$, $p = 0.50$; $n = 9$; Fig. 5B,C). Therefore, the reduction of gamma rhythms likely reflects GABA_BR activation at GC-to-MC synapses (Isaacson and Vitten, 2003; Valley et al., 2013) that are unaltered by our conditional knock-out approach (Fig. 2G). In contrast to gamma oscillations, baclofen strongly decreased spontaneous beta oscillations in WT animals, but not in AOC^{GABAB-/-} mice (respectively, $-54.0 \pm 6.9\%$, $n = 21$ and $-17.8 \pm 7.0\%$, $n = 29$, $F_{(1,48)} = 9.60$, $p < 0.005$, Fisher LSD *post hoc* test: $p < 0.05$ in WT and $p = 0.08$ in AOC^{GABAB-/-}; vehicle in WT: $-7.2 \pm 3.6\%$, $p = 0.50$, $n = 9$; Fig. 5B,C). Therefore, presynaptic GABA_BR activation on cortico-bulbar inputs regulates spontaneous beta but not gamma oscillations in the OB.

AOC feedforward inhibition of odor-evoked M/T activity is depressed by GABA_BR activation

We next investigated the impact of GABA_BR activation at AOC axons on sensory-evoked activity in M/T cells. By stimulating AOC axons during odor presentation, we analyzed the effects of

light stimuli on odor-evoked responses (Fig. 6A). We used frequencies of 10, 33, and 67 Hz to deliver light pulses because these frequencies recruit distinct degree of inhibition (Fig. 3F) and correspond to different regimes of cortical activities (respectively theta, beta, and gamma). Figure 6B shows an example M/T cell response to odor and simultaneous odor + light stimulation at baseline or in the presence of baclofen.

Across the population of M/T cells, odor stimulation resulted in either excitation or inhibition in awake mice ($n = 16$ and $n = 24$ odor-unit pairs, respectively, six mice; Fig. 6C,D). Baclofen application had no effect on the population response ($-1.76 \pm 4.19\%$; two-way ANOVA: baclofen \times stimulation: $F_{(3,117)} = 12.92$, $p < 0.0001$; Sidak's multiple-comparisons test: $p = 0.99$; $n = 40$; Fig. 6E). Simultaneous odor + light stimulation produced a significant decrease in odor-evoked M/T cell firing activity at light frequencies of 33 and 67 Hz, whereas 10 Hz light stimulation did not alter the neuron's evoked activity (one-way ANOVA: $F_{(3,72,144.9)} = 22.4$, $p < 0.0001$; Holm-Sidak's multiple-comparisons test: $p = 0.061$ for 10 Hz, $p < 0.0001$ for 33 and 67 Hz stimulation; $n = 40$; Fig. 6Di,Dii,Diii), regardless of whether the odor was excitatory or inhibitory ($p > 0.05$ at 10 Hz and $p <$

0.0001 at 33 and 67 Hz for both odor responses, $n = 16$ and $n = 24$, respectively; Fig. 6E). The light-induced inhibition of M/T cell odor-evoked activity was diminished with baclofen for both 33 and 67 Hz stimulation, whereas baclofen had no effect on 10 Hz light stimulation (baclofen-induced diminution of light inhibition: 10 Hz: $-3.1 \pm 4.2\%$, 33 Hz: $-34.4 \pm 5.4\%$, 67 Hz: $-12.3 \pm 6.2\%$; baclofen $F_{(1,39)} = 4.38$, $p < 0.043$, baclofen \times stimulation: $F_{(3,117)} = 12.92$, $p < 0.0001$; $p = 0.92$, $p < 0.0001$ and $p < 0.05$ at 10, 33 and 67 Hz; $n = 40$; Fig. 6E). When separately analyzing odor-inhibited and odor-excited neurons, we observed that, for odor-inhibited responses, baclofen depressed the inhibition of M/T cell activity induced by simultaneous odor and light application at 33 or 67 Hz. For odor-excited responses, baclofen produced a significant decrease in M/T cell inhibition only when odor stimulation was paired with 33 Hz light (odor-inhibited neurons: $F_{(1,23)} = 29.0$, $p < 0.0001$, baclofen \times stimulation: $F_{(3,69)} = 27.9$, $p < 0.0001$; $p < 0.0001$ for 33 and 67 Hz, $n = 24$; odor-excited neurons: $F_{(1,15)} = 0.67$, $p = 0.043$, baclofen \times stimulation: $F_{(3,45)} = 36.1$, $p < 0.0001$; $p < 0.01$ for 33 Hz and $p = 0.49$ for 67 Hz, $n = 16$). Therefore, in the context of odor-evoked M/T cell activity, GABA_BR activation at AOC axon terminals depresses the cortico-bulbar inhibition on M/T cells.

To confirm the impact of cortical GABA_BR presynaptic activation on odor-evoked activity of the M/T cell population, we performed calcium imaging in freely behaving animals using fiber photometry (Fig. 7A). To specifically record M/T cell Ca²⁺ transients, we injected a Cre-dependent AAV expressing GCaMP6f (Chen et al., 2013) in the dorsolateral region of Tbet-Cre mice OBs (Haddad et al., 2013). GCaMP6f was excited continuously at low intensity (0.4–0.5 mW) and the volume fluorescence was collected using an optic fiber implanted above the injection site, spectrally separated using a dichroic mirror, and emission intensity was measured with a femtowatt photodetector (Fig. 7A,B). To gain independent light control of AOC axons and to avoid cross-excitation between GCaMP6f and ChR2, we injected the red-shifted channelrhodopsin ChRimson (Klapeetke et al., 2014) into the AOC and targeted red light stimulation above the AOC, which was connected to a 589 nm laser (Fig. 7A,B). Using this technique, AOC light stimulation at 10, 33, or

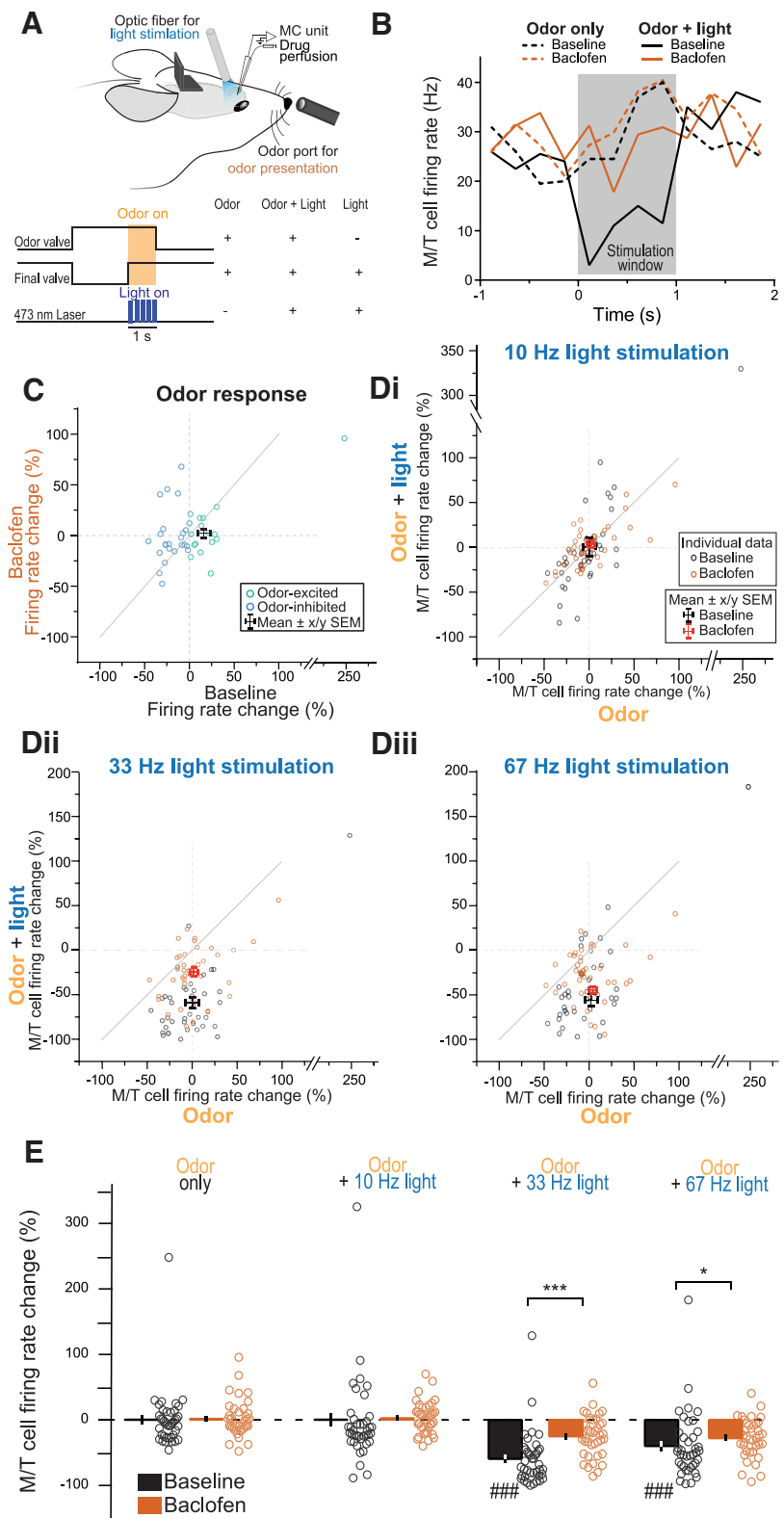


Figure 6. GABA_BR activation at AOC axons diminishes the light-induced inhibition of M/T cell odor-evoked activity. **A**, Top, Schematic drawing showing light delivery and odor presentation to the animal's nose while recording M/T cell activity in awake mice. Bottom, Timing of the stimuli presentation. Light and/or odor were alternatively presented for 1 s. The final valve always opened at the onset of stimulation even in light-only trials. **B**, Example cell's response to odor and simultaneous odor and light presentation in baseline and baclofen conditions. **C**, Odor response of individual neuron–odor pair ($n = 40$) in baseline and baclofen conditions. **D**, Firing rate change of neuron–odor pairs ($n = 40$) to odor only or simultaneous odor and light presentation at 10 (**Di**), 33 (**Dii**), or 67 Hz (**Diii**). **E**, Summary of the impact of 10, 33, or 67 Hz light stimulation on odor-evoked activity of individual neuron–odor pair in baseline and baclofen conditions. Black and red crosses represent the mean \pm x and y SEM. ### $p < 0.0001$ with a Holm–Sidak's multiple-comparisons test after one-way ANOVA; * $p < 0.05$ and *** $p < 0.001$ with a Sidak's multiple-comparisons test after two-way ANOVA.

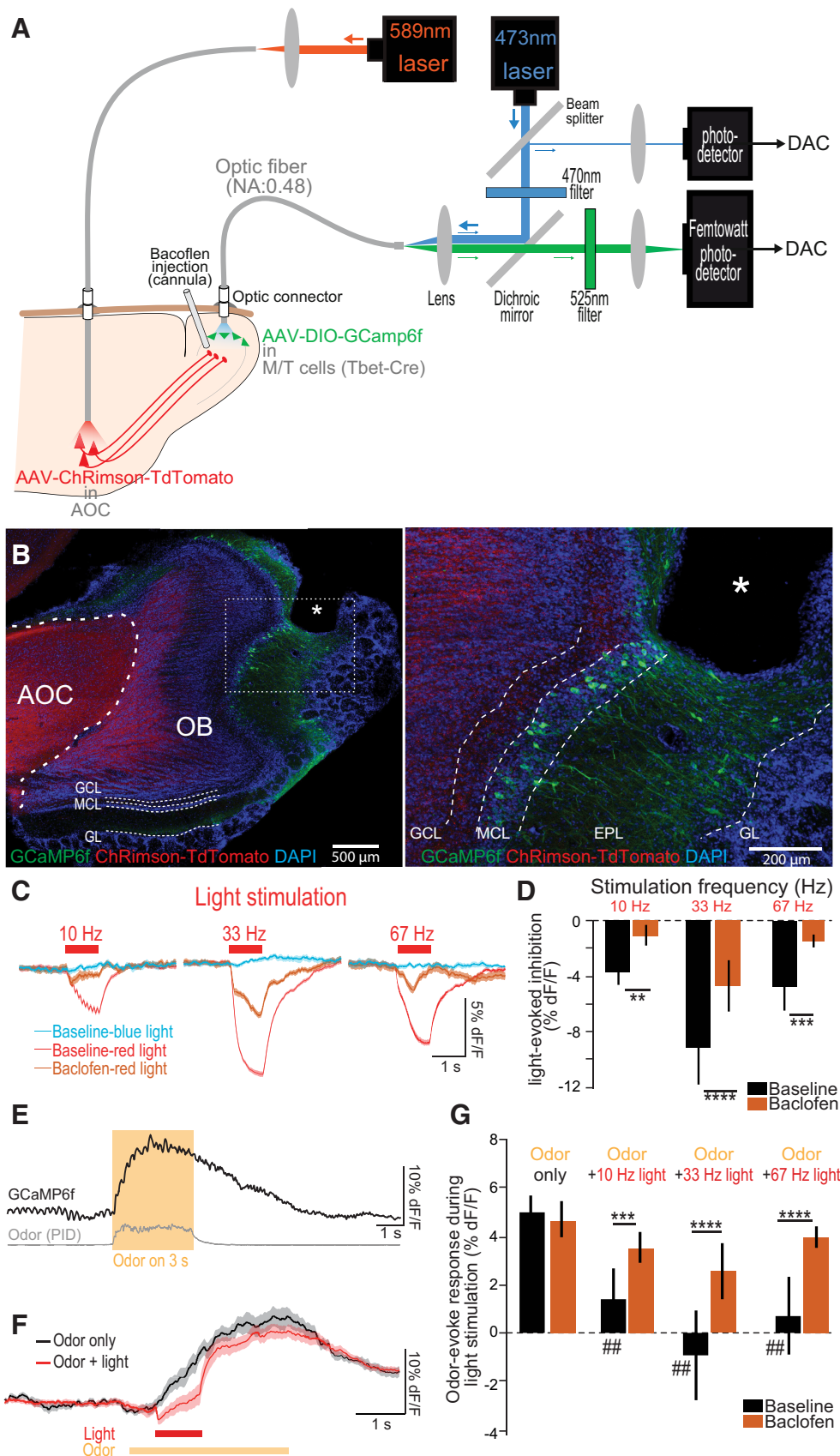


Figure 7. Fiber photometry of Ca^{2+} dynamics reveals that light-induced inhibition of M/T cell odor-evoked activity is reduced by $GABA_B$ activation. **A**, Schematic of the experimental paradigm using fiber photometry. Conditional $GCaMP6f$ expression in $Tbet-Cre$ mice was restricted to M/T cells. Light path for $GCaMP6f$ fluorescence excitation and emission was through a single $400 \mu m$ fiber optic (NA 0.48) connected to an implanted optic fiber targeting the dorsolateral part of the OB. The red-shifted channelrhodopsin $ChRimson$ was expressed in AOC neurons and light activated using an optic fiber implanted above the injection site and connected to a 589 nm laser. **B**, Confocal images showing $ChRimson$ expression in AOC axons and $GCaMP6f$ (Figure legend continues.)

67 Hz with red light (589 nm, 5–10 mW) produced a global reduction of spontaneous fluorescence at the recording site ($\Delta F/F$: $-3.7 \pm 0.9\%$ at 10 Hz, $-9.2 \pm 2.7\%$ at 33 Hz, and $-4.8 \pm 0.7\%$ at 67 Hz, $n = 6$; Fig. 7C), confirming the sensitivity of fiber photometry to detect a population decrease in Ca^{2+} transients during spontaneous activity in freely behaving mice. These effects were not observed when using blue light (473 nm) at the intensity used for GCaMP6f excitation (0.4–0.5 mW), validating the absence of cross-excitation between ChR2 and GCaMP6f (Fig. 7C). With local OB infusion of baclofen, this inhibition was reduced (two-way ANOVA: baclofen $F_{(1,5)} = 13.05$, $p = 0.015$, Holm–Sidak’s multiple-comparisons test: $p < 0.01$ for all light frequencies; Fig. 7C,D). Upon odor presentation, M/T cell responses were characterized by a strong elevation in fluorescence superimposed on a robust breathing modulation of the signal (Fig. 7E). We observed an increase in the GCaMP6f signal in all the odor-recording site pairs in basal conditions (Fig. 7F) and these odor-evoked transients remained unchanged in presence of baclofen (baseline: $+4.9 \pm 0.8\%$, baclofen: $+4.7 \pm 0.7\%$; paired t test: $p = 0.69$; $n = 15$; Fig. 7G). When the AOC was light stimulated in addition to odor presentation, we observed a decrease in the M/T cell odor-driven responses (one-way ANOVA: $F_{(1,461,20,46)} = 13.25$, $p = 0.0006$, Holm–Sidak’s multiple-comparisons test: $p < 0.01$ for 10, 33, and 67 Hz frequencies, $n = 15$; Fig. 7G). Similar to the electrophysiological recordings, we found that baclofen depressed the light-induced reduction of M/T cell odor-evoked activity and this effect was significant at all frequencies (baclofen: $F_{(1,14)} = 4.7$, $p = 0.048$, baclofen \times stimulation: $F_{(2,28)} = 1.9$, $p < 0.17$, $p < 0.001$ *post hoc* for 10, 33, and 67 Hz frequencies, $n = 15$; Fig. 7G). Together with our *in vivo* electrophysiological recordings, these data show that activation of presynaptic GABA_BRs at AOC axon terminals profoundly remodels M/T cell responses to simultaneous sensory and top-down inputs.

Discussion

Cortical projections influence olfactory information processing as early as in the first central relay of the olfactory system, namely the OB. In this region, cortico-bulbar feedback transfers information about, for example, brain states, attention, and prior sensory experience. Because these top-down inputs convey signals relative to dynamic internal states, their regulation must be an essential feature for their precise function. In this study, we revealed a GABA_BR-dependent mechanism to modulate cortico-bulbar feedback. Using a combination of genetics, pharmacology, electrophysiology, and Ca^{2+} imaging of neuronal population, we found that: (1) activation of presynaptic GABA_BRs reduces the direct glutamatergic inputs

onto GCs, but not M/T cells; (2) GABA_BR activation blocks cortical-driven feedforward inhibition of M/T cells’ spontaneous and odor-evoked firing activity; (3) GABA_BR activation biases M/T cell excitatory/inhibitory response ratio to cortical stimulation toward excitation; and (4) depressing glutamate release from AOC axons reduces beta, but not gamma oscillations. Interestingly, GABA_BR activation does not shunt the overall AOC feedback to the OB, but instead refines the functional connectivity between the AOC and OB.

In this study, we introduced ChR2 into the two olfactory primary cortices, the AON and APC, to gain control over the main source of cortico-bulbar projections. Despite the anatomical distinction of the two olfactory cortices, there is no clear evidence that they affect OB function differentially. Both areas mainly target the GCL and GL of the OB (Boyd et al., 2012; Markopoulos et al., 2012; Lepousez et al., 2014) and, even though distinction in the precise connectivity patterns seems to exist, such subtle differences can also be found within specific area subdivisions (Haberly and Price, 1978a, 1978b; Davis and Macrides, 1981). Moreover, recent studies investigating either AON or APC inputs reported a comparable connectivity pattern (NBQX-sensitive inputs to GCs, MCs, and GL neurons such as periglomerular neurons and superficial short axon cells) and similar functional impact on M/T cell odor-evoked responses (Boyd et al., 2012; Markopoulos et al., 2012). Therefore, we chose here to consider the AON and APC as a single functional entity that we collectively named the anterior (primary) olfactory cortex (or AOC). Further work would be required to investigate potential differences in top-down functions of AON and APC.

GABA_BRs are widely expressed in the OB. In addition to cortico-bulbar terminals, GABA_BRs are expressed at olfactory sensory neuron terminals to depress glutamate release. Sensory inputs drive M/T cell activity (Cang and Isaacson, 2003; Margrie and Schaefer, 2003; Phillips et al., 2012) and generate theta OB oscillations (for review, see Kay et al., 2009). In our condition, neither M/T cell spontaneous firing rate nor theta rhythms was sensitive to local baclofen infusion in the GCL. Therefore, it seems apparent that baclofen did not diffuse superficially to sensory axon terminals in the GL. Recordings of fEPSPs at different depths in the GCL further confirmed the drug diffusion area to be $< 600 \mu\text{m}$. GABA_BRs are also expressed at GC apical dendrites, where they depress GABA release, as reported *in vitro* (Isaacson and Vitten, 2003; Valley et al., 2013). Surprisingly, we did not observe any effect of baclofen on light-evoked feedforward inhibition onto M/T cells in AOC^{GABAB^{-/-}} mice (Fig. 3F). Given the remoteness of the virus injection site to the OB, the unaltered GABA_BR1 immunoreactivity in the EPL of AOC^{GABAB^{-/-}} mice and with the near absence of labeled GCs in the OB, it is highly unlikely that the virus diffused to the OB and altered GABA_BR expression at GC dendrites. Moreover, spontaneous gamma oscillations, which rely on dendrodendritic reciprocal synapses (Rall and Shepherd, 1968; Lepousez and Lledo, 2013), were strongly reduced after GABA_BR activation in AOC^{GABAB^{-/-}}. Therefore, the lack of effect of baclofen on M/T cell feedforward inhibition in AOC^{GABAB^{-/-}} mice suggests that distal stimulation of GCs by M/T cell dendrites triggers GABA_BR-sensitive GABA release, whereas AOC terminal proximal stimulation of GCs triggers GABA release in a GABA_BR-independent manner. An alternate hypothesis could be that AOC axon stimulation preferentially engages adult-born GCs, which have been proven to be GABA_BR insensitive (Valley et al., 2013). In any case, because GABA_BR activation had no effect in AOC^{GABAB^{-/-}} mice, we further reasoned that AOC inputs trigger feedforward inhibi-

←

(Figure legend continued.) in M/T cells. Right, Higher-magnification image showing the track of the implanted 400 μm optic fiber above intact GCaMP6f-expressing M/T cells and dendrites in the dorsolateral part of the OB. **C**, Average photometry traces (mean \pm SE, average of 10 traces) in baseline with red (589 nm, 5–10 mW) or blue light stimulation (473 nm, 0.4–0.5 mW) and in baclofen with red light stimulation (589 nm, 5–10 mW). **D**, Summary of fluorescence changes during light stimulation in baseline and baclofen conditions ($n = 6$). **E**, Representative individual trace showing M/T cell fluorescence changes with odor presentation. Note the breathing modulation on top of the odor-evoked response. Odor dynamic was measured using a PID. **F**, Average photometry traces (mean \pm SE, average of 10 traces) with odor presentation (black) and with odor + 33 Hz light stimulation (red) in baseline condition. **G**, Summary of odor- and odor + light-evoked changes in M/T cell fluorescence across all odor-recording pairs ($n = 15$). ## $p < 0.01$, comparing odor and odor + light responses with a Holm–Sidak’s multiple-comparisons test after one-way ANOVA, ** $p < 0.01$, *** $p < 0.001$, **** $p < 0.0001$ with a Sidak’s multiple-comparisons test after two-way ANOVA.

tion but do not drive significant dendrodendritic recurrent inhibition between M/T cells.

To our knowledge, the present study is the first to show the presence of GABA_BRs in a cortico-bulbar synapse. Using selective GABA_BR knock-down in cortico-bulbar projections, we discovered an additional site of GABA_BR expression that adds more insight into the understanding of GABA_BR-dependent modulation of OB activity. We showed that activation of presynaptic GABA_BRs depresses the AOC-to-GC excitatory synapse, thereby blocking AOC-driven feedforward inhibition onto M/T cells. In contrast, we did not find any evidence for GABA_BR-dependent modulation of the AOC-to-M/T cell synapse. The target-dependent expression of presynaptic GABA_BR could reflect the diversity of AOC-projecting cells or it could be determined by the activity or the nature of the postsynaptic target (i.e., glutamatergic or GABAergic), as reported in cultured hippocampal neurons (Schinder et al., 2000). This target-dependent functional expression of GABA_BRs modifies the balance between cortical excitation and feedforward inhibition received by M/T cells. Because the temporal window M/T cells use to integrate cortical excitatory events is tightly controlled by GABA_BR-sensitive feedforward inhibition, GABA_BR activation enlarges this integration windows as observed in thalamo-cortical feedforward circuits (Chittajallu et al., 2013). Using patterned light stimulation of cortico-bulbar inputs at different frequencies, we observed that this differential GABA_BR sensitivity extends the coupling between M/T cell responses and AOC axon stimulations to beta frequencies (10–50 Hz; Fig. 3F). Given that cortical activity can operate at such rhythms, we propose that GABA_BR modulation participates in gating the transfer of the beta regimes on M/T cell firing activity. Consistent with this, we found that GABA_BR activation at cortico-bulbar inputs selectively depresses spontaneous beta oscillations.

Recent evidence suggests a role for top-down inputs on temporal activity of the targeted structure. Top-down inputs might affect ongoing oscillations, synchronicity of postsynaptic cells, and coherence between brain areas (Engel et al., 2001). In the olfactory system, by acting at the AOC axon terminals, we demonstrated that GABA_BRs are well positioned to regulate coherence between distant structures, such as the AOC and the OB, a phenomenon likely to emerge in behaviorally relevant tasks (Chabaud et al., 1999; Kay and Beshel, 2010; Cohen et al., 2015). In particular, beta oscillations were depressed by cortical GABA_BR activation and have been proposed to be supported by a reentry of cortical input in the OB (Gray and Skinner, 1988; Neville and Haberly, 2003; Martin et al., 2014). GABA_BR could thereby regulate the shift in coherence between cortical structures and the OB under different sensory experiences (adaptation, learning, memory, etc.). In the near future, it will be of great interest to investigate the behavioral impact of this GABA_BR-dependent presynaptic modulation of top-down activity and to decipher in which context it is engaged.

References

- Balu R, Pressler RT, Strowbridge BW (2007) Multiple modes of synaptic excitation of olfactory bulb granule cells. *J Neurosci* 27:5621–5632. [CrossRef Medline](#)
- Boyd AM, Sturgill JF, Poo C, Isaacson JS (2012) Cortical feedback control of olfactory bulb circuits. *Neuron* 76:1161–1174. [CrossRef Medline](#)
- Boyd AM, Kato HK, Komiyama T, Isaacson JS (2015) Broadcasting of cortical activity to the olfactory bulb. *Cell Rep* 10:1032–1039. [CrossRef Medline](#)
- Cang J, Isaacson JS (2003) In vivo whole-cell recording of odor-evoked synaptic transmission in the rat olfactory bulb. *J Neurosci* 23:4108–4116. [Medline](#)
- Chabaud P, Ravel N, Wilson DA, Gervais R (1999) Functional coupling in rat central olfactory pathways: a coherence analysis. *Neurosci Lett* 276:17–20. [CrossRef Medline](#)
- Chen T-W, Wardill TJ, Sun Y, Pulver SR, Renninger SL, Baohan A, Schreier ER, Kerr RA, Orger MB, Jayaraman V, Looger LL, Svoboda K, Kim DS (2013) Ultrasensitive fluorescent proteins for imaging neuronal activity. *Nature* 499:295–300.
- Chittajallu R, Pelkey KA, McBain CJ (2013) Neurogliaform cells dynamically regulate somatosensory integration via synapse-specific modulation. *Nat Neurosci* 16:13–15. [CrossRef Medline](#)
- Cohen Y, Putrino D, Wilson DA (2015) Dynamic cortical lateralization during olfactory discrimination learning. *J Physiol* 593:1701–1714. [CrossRef Medline](#)
- Davis BJ, Macrides F (1981) The organization of centrifugal projections from the anterior olfactory nucleus, ventral hippocampal rudiment, and piriform cortex to the main olfactory bulb in the hamster: an autoradiographic study. *J Comp Neurol* 203:475–493. [Medline](#)
- Engel AK, Fries P, Singer W (2001) Dynamic predictions: oscillations and synchrony in top-down processing. *Nat Rev Neurosci* 2:704–716. [CrossRef Medline](#)
- Franks KM, Russo MJ, Sosulski DL, Mulligan AA, Siegelbaum SA, Axel R (2011) Recurrent circuitry dynamically shapes the activation of piriform cortex. *Neuron* 72:49–56. [CrossRef Medline](#)
- Gray CM, Skinner JE (1988) Centrifugal regulation of neuronal activity in the olfactory bulb of the waking rabbit as revealed by reversible cryogenic blockade. *Exp Brain Res* 69:378–386. [Medline](#)
- Gunaydin LA, Grosenick L, Finkelstein JC, Kauvar IV, Fenno LE, Adhikari A, Lammel S, Mirzabekov JJ, Airan RD, Zalocusky KA, Tye KM, Anikeeva P, Malenka RC, Deisseroth K (2014) Natural neural projection dynamics underlying social behavior. *Cell* 157:1535–1551. [CrossRef Medline](#)
- Haberly LB, Price JL (1978a) Association and commissural fiber systems of the olfactory cortex of the rat. II Systems originating in the olfactory peduncle. *J Comp Neurol* 181:781–807. [CrossRef Medline](#)
- Haberly LB, Price JL (1978b) Association and commissural fiber systems of the olfactory cortex of the rat. I. Systems originating in the piriform cortex and adjacent areas. *J Comp Neurol* 178:711–740. [CrossRef Medline](#)
- Haddad R, Lanjuin A, Madisen L, Zeng H, Murthy VN, Uchida N (2013) Olfactory cortical neurons read out a relative time code in the olfactory bulb. *Nat Neurosci* 16:949–957. [CrossRef Medline](#)
- Haller C, Casanova E, Müller M, Vacher CM, Vigot R, Doll T, Barbieri S, Gassmann M, Bettler B (2004) Floxed allele for conditional inactivation of the GABAB(1) gene. *Genesis* 40:125–130. [CrossRef Medline](#)
- Isaacson JS, Strowbridge BW (1998) Olfactory reciprocal synapses: dendritic signaling in the CNS. *Neuron* 20:749–761. [CrossRef Medline](#)
- Isaacson JS, Vitten H (2003) GABA(B) receptors inhibit dendrodendritic transmission in the rat olfactory bulb. *J Neurosci* 23:2032–2039. [Medline](#)
- Kay LM, Beshel J (2010) A beta oscillation network in the rat olfactory system during a 2-alternative choice odor discrimination task. *J Neurophysiol* 104:829–839. [CrossRef Medline](#)
- Kay LM, Beshel J, Brea J, Martin C, Rojas-Libano D, Kopell N (2009) Olfactory oscillations: the what, how and what for. *Trends Neurosci* 32:207–214. [CrossRef Medline](#)
- Klapoetke NC, Murata Y, Kim SS, Pulver SR, Birdsey-Benson A, Cho YK, Morimoto TK, Chuong AS, Carpenter EJ, Tian Z, Wang J, Xie Y, Yan Z, Zhang Y, Chow BY, Surek B, Melkonian M, Jayaraman V, Constantine-Paton M, Wong GK, et al. (2014) Independent optical excitation of distinct neural populations. *Nat Methods* 11:338–346. [CrossRef Medline](#)
- Lepousez G, Lledo PM (2013) Odor discrimination requires proper olfactory fast oscillations in awake mice. *Neuron* 80:1010–1024. [CrossRef Medline](#)
- Lepousez G, Nissant A, Bryant AK, Gheusi G, Greer CA, Lledo PM (2014) Olfactory learning promotes input-specific synaptic plasticity in adult-born neurons. *Proc Natl Acad Sci U S A* 111:13984–13989. [CrossRef Medline](#)
- Linster C, Fontanini A (2014) Functional neuromodulation of chemosensation in vertebrates. *Curr Opin Neurobiol* 29:82–87. [CrossRef Medline](#)
- Ma M, Luo M (2012) Optogenetic activation of basal forebrain cholinergic neurons modulates neuronal excitability and sensory responses in the main olfactory bulb. *J Neurosci* 32:10105–10116. [CrossRef Medline](#)
- Manabe H, Kusumoto-Yoshida I, Ota M, Mori K (2011) Olfactory cortex

- generates synchronized top-down inputs to the olfactory bulb during slow-wave sleep. *J Neurosci* 31:8123–8133. [CrossRef Medline](#)
- Margeta-Mitrovic M, Mitrovic I, Riley RC, Jan LY, Basbaum AI (1999) Immunohistochemical localization of GABA(B) receptors in the rat central nervous system. *J Comp Neurol* 405:299–321. [CrossRef Medline](#)
- Margrie TW, Schaefer AT (2003) Theta oscillation coupled spike latencies yield computational vigour in a mammalian sensory system. *J Physiol* 546:363–374. [CrossRef Medline](#)
- Markopoulos F, Rokni D, Gire DH, Murthy VN (2012) Functional properties of cortical feedback projections to the olfactory bulb. *Neuron* 76:1175–1188. [CrossRef Medline](#)
- Martin C, Ravel N (2014) Beta and gamma oscillatory activities associated with olfactory memory tasks: different rhythms for different functional networks? *Front Behav Neurosci* 8:218. [CrossRef Medline](#)
- Martin C, Gervais R, Messaoudi B, Ravel N (2006) Learning-induced oscillatory activities correlated to odour recognition: a network activity. *Eur J Neurosci* 23:1801–1810. [CrossRef Medline](#)
- Matsutani S, Yamamoto N (2008) Centrifugal innervation of the mammalian olfactory bulb. *Anat Sci Int* 83:218–227. [CrossRef Medline](#)
- Neville KR, Haberly LB (2003) Beta and gamma oscillations in the olfactory system of the urethane-anesthetized rat. *J Neurophysiol* 90:3921–3930. [CrossRef Medline](#)
- Otazu GH, Chae H, Davis MB, Albeanu DF (2015) Cortical feedback decorrelates olfactory bulb output in awake mice. *Neuron*:1–17.
- Petzold GC, Hagiwara A, Murthy VN (2009) Serotonergic modulation of odor input to the mammalian olfactory bulb. *Nat Neurosci* 12:784–791. [CrossRef Medline](#)
- Phillips ME, Sachdev RN, Willhite DC, Shepherd GM (2012) Respiration drives network activity and modulates synaptic and circuit processing of lateral inhibition in the olfactory bulb. *J Neurosci* 32:85–98. [CrossRef Medline](#)
- Poo C, Isaacson JS (2009) Odor representations in olfactory cortex: “sparse” coding, global inhibition, and oscillations. *Neuron* 62:850–861. [CrossRef Medline](#)
- Rall W, Shepherd GM (1968) Theoretical reconstruction of field potentials and dendrodendritic synaptic interactions in olfactory bulb. *J Neurophysiol* 31:884–915. [Medline](#)
- Schinder AF, Berninger B, Poo M (2000) Postsynaptic target specificity of neurotrophin-induced presynaptic potentiation. *Neuron* 25:151–163. [CrossRef Medline](#)
- Shea SD, Katz LC, Mooney R (2008) Noradrenergic induction of odor-specific neural habituation and olfactory memories. *J Neurosci* 28:10711–10719. [CrossRef Medline](#)
- Soria-Gómez E, Bellocchio L, Reguero L, Lepousez G, Martin C, Bendahmane M, Ruehle S, Remmers F, Desprez T, Matias I, Wiesner T, Cannich A, Nissant A, Wadleigh A, Pape HC, Chiarlone AP, Quarta C, Verrier D, Vincent P, Massa F, et al. (2014) The endocannabinoid system controls food intake via olfactory processes. *Nat Neurosci* 17:407–415. [CrossRef Medline](#)
- Valley MT, Henderson LG, Inverso SA, Lledo PM (2013) Adult neurogenesis produces neurons with unique GABAergic synapses in the olfactory bulb. *J Neurosci* 33:14660–14665. [CrossRef Medline](#)
- Youngstrom IA, Strowbridge BW (2015) Respiratory modulation of spontaneous subthreshold synaptic activity in olfactory bulb granule cells recorded in awake, head-fixed mice. *J Neurosci* 35:8758–8767. [CrossRef Medline](#)